

Passing Efficiency of a Low Turbulence Inlet (PELTI)

Final Report to NSF

Prepared by the LTI Assessment Working Group:

Barry J. Huebert¹, Chair

Steven G. Howell¹

David Covert²

Antony Clarke¹

James R. Anderson³

With Collaborating Authors

Bernard G. Lafleur⁴

Russ Seebaugh⁴

James Charles Wilson⁴

Dave Gesler⁴

Darrel Baumgardner⁵

Byron Blomquist¹

¹ Department of Oceanography, University of Hawaii, Honolulu, HI 96822

² Atmospheric Science Dept, JISAO GJ-40, University of Washington, Seattle, WA 98195

³ Mechanical and Aerospace Engineering, Arizona State University, Tempe, AZ 85287

⁴ Department of Engineering, University of Denver, Denver, CO 80208

⁵ Centro de Ciencias de la Atmósfera – UNAM, Universidad Nacional Autónoma de México, Circuito Exterior s/n, Ciudad Universitaria, 04510 México City (D.F.)

Address inquiries to: huebert@soest.hawaii.edu

13 September, 2000

Disclaimer: The data on which this report is based was collected in July, 2000. This report is being submitted in September, 2000. It commonly takes multiple years for investigators to process, quality-check, and publish data from flight programs of this complexity. In view of the extremely short time from data collection to report, perhaps it is reasonable for the authors to attach a “preliminary” label to the tables and plots herein. Some errors will no doubt be discovered and corrected. However, we are confident that they would not change the fundamental conclusions about the functioning of the LTI.

Table of Contents

3	Executive Summary
	Report Summary
4	A. Introduction
5	B. Approach
6	C. LTI Modeled Performance
6	D. Observations
10	E. Conclusions
11	Summary Figures
	1. Introduction
15	1.1 State of the Science
16	1.2 PELTI
	2. Methods
17	2.1 Overall Approach
19	2.2 LTI Configuration
20	2.3 Location of Inlets, Plumbing, and Layout
21	2.4 Bulk Chemical Analyses
22	2.5 SEM Analyses
23	2.6 Aerodynamic Particle Size Measurements
24	2.7 FSSP-300 Observations
25	2.8 Nephelometers
	3. Results
26	3.1 Flight Operations
28	3.2 LTI Aerodynamic Performance
30	3.3 Bulk Filter Data
32	3.4 SEM Data
35	3.5 APS Data
37	3.6 FSSP-300 Measurements
38	3.7 Lab Measurements of Losses in Tubing
39	3.8 Modeling of Enhancements using Fluent
42	3.9 Nephelometers
	Discussion and Critiques of Methods
43	4.1 Tasks Remaining
43	4.2 Critique of APS Data – D. Covert
44	4.3 Critique of Anion and Cation Data – B. Huebert
45	4.4 Sources of Error in SEM Analyses – J. Anderson
46	4.5 FSSP Data Concerns – A. Clarke
48	4.6 Net LTI Passing Efficiency – J. C. Wilson
49	4.7 What Does Particle Size Mean? – S. Howell
	Recommendations and Conclusions
52	5.1 Comparisons of Inlets
53	5.2 Comparisons to Ambient Concentrations
54	5.3 Recommendations
54	References
57	Figures

Executive Summary

In July, 2000 we tested the new porous-diffuser low-turbulence inlet (LTI), developed at the University of Denver, by flying it and three other inlets on NCAR's C-130 in the Caribbean, using both dust and sea salt as test aerosols. Aerosols were analyzed using bulk chemical analysis of ions on filters, scanning electron microscopy (SEM) of filters, TSI aerodynamic particle sizers (APSs), and FSSP-300 (300) optical particle counters.

We found that the LTI consistently admitted more particles to the airplane than did either the NCAR Community Aerosol Inlet (CAI) or a shrouded solid-diffuser/curved-tube inlet (SD). APS size distributions behind the other inlets began to diverge from LTI values above 1-3 μm , with mass concentrations of larger particles lower by as much as a factor of ten behind the CAI and a factor of 2 behind the SD. Modeling of particle trajectories in the LTI with Fluent predicts less than a factor of two enhancement of particles between a few and 7 microns. This was supported by the SEM analyses of particles behind the LTI and TAS.

Comparisons of bulk chemistry with an external reference total aerosol sampler (TAS) found no significant differences between the LTI and TAS, but both the SD and CAI passed lower values for most of the ions analyzed. Thus, the LTI filters can be used to determine the ambient mass mixing ratios of the analyzed ions. The inertial enhancements in the LTI diffuser and estimates of losses in transport to the LTI filter must be taken into account to accurately infer ambient concentrations based on LTI sampling. When this is done, the ambient mass mixing ratios estimated from the LTI filters agree within 20% with the mixing ratios determined from the TAS filters.

Relative to the LTI, the SD and CAI transmission efficiencies (the concentration in the sample flow divided by the ambient concentration) was lowest for "wet" aerosol (i.e., sea-salt), apparently because salt droplets are more likely than dry dust to stick when they impact on the walls of the other inlets.

We set out to test two hypotheses:

A. The LTI has a demonstrably higher aerosol sampling or transmission efficiency than both the CAI (the NCAR C-130 community aerosol inlet) and traditional solid diffusers for particles in the 1-7 μm range.

This hypothesis could not be falsified. All the chemical and physical evidence indicates that the LTI admits more particle mass in this range than the other inlets do.

However, we note that our real goal is to achieve efficiencies near unity. The ubiquity of losses in earlier inlets lead us initially to state this hypothesis in terms of "higher" efficiency, but enhancement by the LTI may cause efficiencies substantially above 1 for particles larger than 3-5 μm . Since enhancements in laminar flow are calculable, most measurements can be corrected for them.

B. It is possible, using the LTI, to sample and characterize the number-size and surface area-size distributions of ambient dust and seasalt inside an aircraft with enough accuracy that uncertainties arising from inlet losses will contribute less than 20% to the assessment of radiative impacts.

This hypothesis also could not be falsified. It essentially asks how well aerosol size distributions behind the LTI represent ambient particle distributions and light scattering. The LTI bulk chemical concentrations were statistically identical to the TAS bulk concentrations of Na^+ , Cl^- , SO_4^{2-} , Mg^{++} , and Ca^{++} , which represent the ambient mixing ratios of those species. The SEM analyses showed that the LTI and TAS number concentrations were statistically identical up to 2 μm ; above 2 μm the LTI showed enhancement within model-predicted limits. When Fluent model-derived inertial enhancements associated with the LTI diffuser and losses associated with transport to the LTI filter are taken into consideration, they explain the observed 20% agreement between LTI and TAS.

Corrections for modest but predictable LTI enhancements also provide light scattering assessments that are representative of ambient size distributions up to 7 μm . Additional contributions to scattering from yet larger aerosol are unlikely to approach 20% for realistic aerosol cases. The error in radiative forcing due to positive and negative sampling biases depends both on the transmission efficiency and the fraction of the mass and total optical depth in each size interval. For those sizes that contribute little to the optical depth, a poor transmission efficiency will cause little error in radiative forcing calculations. It is worth noting, however, that over- or under-sampled sizes could still cause significant errors for other issues, such as the computation of deposition fluxes and heterogeneous reaction rates.

CONCLUSION: Our conclusion, therefore, is that the LTI represents a significant advance in our ability to sample populations of large particles from aircraft. Its efficiency is near enough to unity to enable defensible studies of the distributions and impacts of both mineral dust and sea salt. Corrections will need to be applied for enhancement of particles in the 3-7 μm range. We recommend that the ACE-Asia program use LTIs to provide samples to the various aerosol instruments on board the NCAR C-130.

Report Summary

A. Introduction

It has long been known that typical diffuser-and-curved-tube airborne inlet systems remove particles from sampled airstream, so that instruments downstream receive air that has been depleted of supermicron particles. Since most instruments require that air be decelerated from aircraft velocities to a few m/s prior to its analysis, decelerating diffusers have been widely used in airborne sampling. Apparently the highly-turbulent flow just inside the tip of these conical diffusers causes the largest particles to be impacted on the walls of the diffuser. With the possible exception of mineral particles that may bounce off the walls, this has the effect of removing large particles and distorting the particle-size spectrum behind diffusers.

A workshop was convened at NCAR in 1991 to assess the state of knowledge about inlet systems. Attendees concluded that it was not possible at that time to sample supermicron particles from aircraft without substantial and unquantifiable size-dependent negative biases, and made several recommendations for ways to study and improve airborne aerosol inlets (Baumgardner et al., 1991). The notion of a shallow angle diffuser with a shrouded inlet prompted the design of the NASA SD employed in this study. Similarly the NCAR Community Aerosol Inlet (CAI) incorporated several features intended to minimize artifacts. One of the most promising suggestions from the 19901 workshop was that of Denver University researcher Russell Seebaugh, who noted that aerodynamic engineers have for years suppressed turbulence in diffusers by using boundary layer suction to prevent the separation of the boundary layer from the diffuser walls. Since that time, Seebaugh and his colleagues Bernard LaFleur and James C. Wilson have developed that concept in the laboratory. This led to the fabrication of the LTI that is the focus of this report (Figure S1).

B. Approach

Hypothesis A can be tested relatively simply, since it only requires measurements inside the aircraft, on air streams that have already been decelerated. We used three matched aerodynamic particle sizers (TSI Model 3320 APS's) to measure the physical size distribution behind our three test inlets: the LTI, CAI, and SD. The difference between the APS distributions provides a direct test of Hypothesis A. Nephelometers behind each inlet provided a real-time signal in flight to guide the test and a relevant integral measure of light scattering that is appropriate to the tests and one of the goals of ACE-Asia, radiative transfer. We also collected filter samples for chemical analysis behind each of these inlets. That included both Teflon filters for ion-chromatographic analysis of major anions and cations (Barry Huebert's group) and streakers with Nuclepore filters (SEM analyses by Jim Anderson). In dust, Anderson counted and sized the particles behind each inlet with automated SEM (without chemical analysis) that could amass statistics on thousands of particles.

Hypothesis B is considerably more difficult to test, since it involves comparing aerosol distributions behind the LTI to those in ambient air. The crux of the problem is to measure the ambient (reference) distribution with a system that does not itself suffer from inlet or other artifacts. One of the most defensible external references is the bulk concentration of particles, as measured by the TAS designed and built in the NCAR shop. This external sampler permits an analysis of every particle that enters the inlet tip, whether it has been deposited on the inside of the diffuser or collected on its filter. The diffuser is lined by removable cones, which are replaced with each filter sample and extracted after the flights. As long as one samples isokinetically, we can be assured that the sum of the cone extract and its filter contains every particle that entered the TAS tip and is representative of the ambient aerosol concentration. TAS was used to measure reference ambient concentrations of both seasalt and dust. When sampling dust, the size of mineral aerosol was preserved in the TAS extracts (except for aggregates), so that the ambient (TAS) and LTI size distributions could both be measured directly by SEM. Only comparisons utilizing a single physical principal (either SEM or IC analyses) were considered to be valid tests of the LTI.

The FSSP-300 is another external device that seemed to offer the best hope for characterizing the ambient size distribution that could then be compared to a similar probe mounted internally

behind the LTI. However, inconsistencies in the internal FSSP data and uncertainties concerning the nature of the flow in its sample volume led to comparisons that we are unable to reconcile with the other aerosol measurements. It is worth noting that the counting efficiency of 300s in these different configurations has never been calibrated, in contrast to their sizing ability. Hence, we have focussed on the TAS data as our external reference.

C. LTI Modeled Performance

The design of the LTI was expected to lead to some enhancement in larger particles. This occurs when particles with sufficient inertia deviate from the curving streamlines caused by aspirating most of the flow through the sides of the LTI porous diffuser. However, losses of some larger particles in this prototype are caused by the 90 deg bend in the tube behind the inlet (Fig. S1). Fluent calculations that account for these enhancements and losses (Fig S2) indicate that a net enhancement should become evident around $3\mu\text{m}$ and approach about 40% by $6\mu\text{m}$. In the final Figure of this Summary (Fig. S6) we correct for this enhancement

D. Observations

D.1. Aerodynamic Particle Sizers

Aerodynamic Particle Sizers (APS, Model 3320, TSI Inc, St. Paul MN) (Wilson and Liu, 1980) were used to count and size particles according to their aerodynamic diameter, D_{ac} , in the range from 0.8 to $13\mu\text{m}$ downstream of each of the three inlets, the LTI, CAI, and SD. Each APS unit drew its 5 l/min from an identical distribution plenum one of the inlets as described above. The APS measurements were overseen by Steve Howell of UH and Dave Covert, of the University of Washington.

Figure S3 contains two examples of APS volume distribution data from Flight 8 collected concurrently from the LTI, CAI and SD for so called “dry” and “wet” conditions in the presence of coarse aerosol. Note that we plot volume distributions (rather than number) to make factors of two or less differences in the largest sizes evident. “Dry” refers to low relative humidity (RH) conditions common above the marine inversion and in the presence of dry dust aerosol. “Wet” refers to higher RH conditions common to the marine boundary layer where coarse sea-salt is deliquesced into a “wet” saline droplet (although at this low wind speed much of the small mode may be dust). In the “dry” case (Fig S3, Left) at 2100 m altitude the LTI and SD concentrations are similar up to $1.5\mu\text{m}$, after which SD concentrations are about 20% lower than the LTI. However, CAI concentrations are less than 50% of corresponding LTI values. In the “wet” case (Fig. S3, right) at 30 m discrepancies are much greater: SD concentrations are about 60% of LTI values between 2 and $7\mu\text{m}$ while CAI values are far less: about 10-20% of the LTI values over this range.

D.2. Bulk Analysis of Anions and Cations

Filter samplers behind each inlet were compared with data from the Total Aerosol Sampler, TAS. Since TAS enables an analysis of every particle that enters its tip (whether on the Teflon filter or extracted from the interior walls of the inlet cone), it serves as an ambient reference for

other filter samplers. Because analyzing TAS samples involves handling and extracting a cone as well as a filter, the precision of TAS will never be as good as that of a single filter analysis, but its lack of sampling bias means that it has a definable accuracy. Ion chromatography was used to analyze all filters and TAS samples for Cl^- , SO_4^{2-} , Na^+ , Ca^{++} , and Mg^{++} . The major source of uncertainty was the variability of blank concentrations.

Figure S4 compares Cl^- behind all the inlets with TAS Cl^- in the left panel and with LTI Cl^- in the right panel. The LTI concentration is indistinguishable from that of TAS, while the SD and CAI brought considerably less Cl^- into the cabin. We conclude that the LTI reproduces ambient Cl^- concentrations to within at least 20%, in spite of enhancements and losses that may affect the larger end of the sea salt size distribution. The relative behavior of the inlets is clearer when SD and CAI samples are plotted against the LTI in the lower panel. Similar differences were noted for the other ions:

Average Ratios of Species Concentrations Behind Various Inlets to TAS Concentrations

Ratio	Cl	SO4	Na	Mg	Ca	NSS(Mg)
LTI/TAS	1.15	1.03	0.94	0.86	1.03	1.23
Solid/TAS	0.58	0.84	0.54	0.51	0.74	1.32
CFilt/TAS	0.17	0.52	0.20	0.19	0.25	0.86
CImp/TAS	0.16	0.50	0.18	0.19	0.24	0.79

This chemical data suggests that the sea salt and dust modes are sampled with nearly-unit efficiency by the LTI. It also shows a demonstrable lowering of efficiency when the LTI flow was made turbulent rather than laminar. In these cases the majority of the mass distribution was smaller than 4 μm so that LTI enhancement biases were not large.

D.3. Scanning Electron Microscopy

Streaker samplers enabled the collection of Nuclepore filter samples behind each inlet on every flight leg. In addition, on high altitude legs we exposed Nuclepore filters in TAS, so that we had an ambient SEM reference for mineral dust particles. Only about 10% of the dust particles adhered to the TAS cone (dry particles tend to bounce off), so most of the particles did not need to be extracted for analysis. Thus, the SEM enabled comparisons of particle size distributions behind each inlet for comparison with the ambient distribution from TAS.

It should be noted that these size distributions differ from those measured by the APSs. A significant fraction of the large particles were tabular clays, whose complex shapes defy simple descriptions such as diameter. Furthermore, the extra drag of these complex particles would cause them to appear small for their mass in the APS, where the smallest particles tend not to deviate from the path of the air. Ironically, because of their large surface to mass ratio, they would size large for their mass in instruments that measure light scattering. Reconciling these various measurements has given us many insights about ways to study dust particles in ACE-Asia.

Two dust samples from Flight 8 have been extensively analyzed by SEM. As Fig. S5 demonstrates, there is good agreement (<20% in the number distribution) between TAS and the LTI below 2 μm , which suggests that the sampled volumes have been correctly accounted for. Above 2 μm the TAS and LTI distributions in this sample diverge to suggest an enhancement by the LTI of a factor of 2 in the 3-8 μm range. The other sample shows overlap up to about 6 μm and then enhancement by only about 20% up to 8 μm (see full report). This data, which is our most reliable comparison of ambient and internal particle sizes, is in general agreement with the modeling (suggesting a small enhancement) and the ion chemistry (suggesting that the bulk of the sea salt mode is sampled with no more than modest enhancement).

D.4. Nephelometer

The Radiance Research nephelometers (530nm) behind each inlet characterized the integral light scattering of the aerosol from 8 to 168 deg. Larger particles concentrate a greater proportion of their scattered light in the forward direction such that this angular truncation underestimates the scattering contribution of the largest particles. However, we also used a second nephelometer behind the LTI inlet with an aerodynamic size cut near 1 μm to characterize the submicrometer scattering and subtract it from the total to identify coarse scattering only. For the PELTI data discussed here, submicrometer scattering was about 1/3 of the total such that total scatter was dominated by coarse particle scattering in spite of possible truncation losses due to forward scatter from the largest particles. Although the LTI consistently saw higher mass concentrations, light scattering values behind the LTI and SD inlets were virtually the same when compared over the experiment, with leg average differences generally about 13% (see full report for Figure). On the other hand, scattering data behind the CAI was consistently about 40% less than LTI or SD values. The relationship between size and scattering is explored in Section D.6.

D.5. FSSP-300 Wing/Cabin Comparison

Two FSSP-300s were provided by the NCAR Research Aviation Facility and NASA Ames Research Center. Darrel Baumgardner and Jeff Stith oversaw these measurements. The gains of the amplification sections of both probes were adjusted to insure that each probe showed peaks in identical channels for the same calibration aerosol sizes. Small differences in collection angles will make a small contribution to sizing differences and the Gaussian intensity distributions of the two laser beams may cause differences, although the average uncertainty should be similar for the two instruments. There is approximately a 20% uncertainty in determining the size of particles from the FSSP scattered light measurements.

When mounted upon opposite wings both probes generally performed similarly, with flight-leg average concentrations in identical size bins differing by between zero and 300% (Figure 3.6.1 in full report). However, when either probe was mounted inside the C-130 with a sample cavity arrangement designed to maximize sensitivity by focusing the particles into the center of the beam, unexplainable sizing was evident in the cabin probe (see full report Figures 3.6.2 and 3.6.3). Since we are aware of no tests of FSSP counting efficiency in this altered flow configuration and since no consistency was found between the FSSP and any of the other

observations reported above, we cannot defend the internal FSSP distributions as realistic representations of the aerosol from the LTI.

D.6. Impact of Inlets on Optical Properties

The above data (chemistry, SEM, APS, light scattering) clearly show that the LTI passes more aerosol mass than the SD and far more than the CAI. Model results indicate that some of this may arise from enhancements in the transmission of larger aerosol. The light scattering data indicate that for these test aerosols differences between LTI and SD transmission of the optically significant sizes seen by the nephelometers are often similar (<10%) while the CAI transmits only about 60% of optically significant sizes for PELTI conditions. In order to bring these various observations into focus we have taken the “wet” and “dry” cases illustrated above in the APS data for flight 8 and presented them in Figure S6. In view of the large deficiencies of the CAI we will focus on differences between the LTI and shrouded SD inlets. We would prefer to compare with ambient optical properties, but without a measure of optical depth through a layer we have no such reference.

Is the more expensive and complex LTI a significant improvement over a shrouded SD for measuring aerosol optical properties? To answer that we apply the corrections to LTI data for model enhancements shown in Fig. S2 that reduce the original LTI concentrations. (This is now our best guess at ambient properties.) Small corrections are also applied to the SD for large-particle transmission losses. Original and corrected data are shown for both LTI and SD data in Figure S6. Our best estimate of the performance differences are seen in the differences between the bold green (corrected LTI) and bold red (corrected SD) lines. These are plotted as volume distribution, scattering distribution and cumulative scattering for the “dry” and “wet” cases. For the “dry” case the differences in the dry volume distributions are small but do approach about 20% in the 3.5 to 5 μm range where volume is largest for this case. This also shows up as a similar 20% difference in scattering extinction over this size range but because these particle sizes are less efficient at scattering light than smaller particles this is not a region that dominates the scattering distribution. Consequently, the effect on modeled cumulative scattering as size increases only shows about a 6% lower value for the SD when compared to the LTI.

For the “wet” case, differences in corrected SD and LTI aerosol volume is significant between about 1.5 and 6 μm with SD values about 35% lower than LTI values. The associated scattering distributions for this case are similarly lower over the same size range. In this case the LTI effect on cumulative scattering is about 17%, indicating a significant improvement in optical characterization with the LTI. This is somewhat larger than the difference measured by the nephelometers behind the two inlets, but it is dominated by particles larger than 3 μm where nephelometer truncation (9-168deg) error leads to underestimates in scattering compared to modeled results (0-180deg).

E. Conclusions

- The chemical and SEM data that show the LTI is admitting essentially all of the TAS mass.
- The SEM data indicates an enhancement of particles in the 2-8 μm range of a factor of two or less.
- The FLUENT modeling of particle trajectories in the LTI predicts a slight enhancement, reaching 44% in the vicinity of 6 μm .
- In view of these observations, we feel that the LTI is a clear improvement over other inlets and provides a means to characterize ambient optical properties well within the 20% uncertainty that was our goal. Because of the rapid fall-off in scattering efficiency with size, only very large increases in large particle mass with diameters above 7 μm could introduce uncertainties in scattering due to losses through the LTI that might approach 20%.

Details of the methods, figures showing much of the data, and a critique of each method are all contained in the full Report.

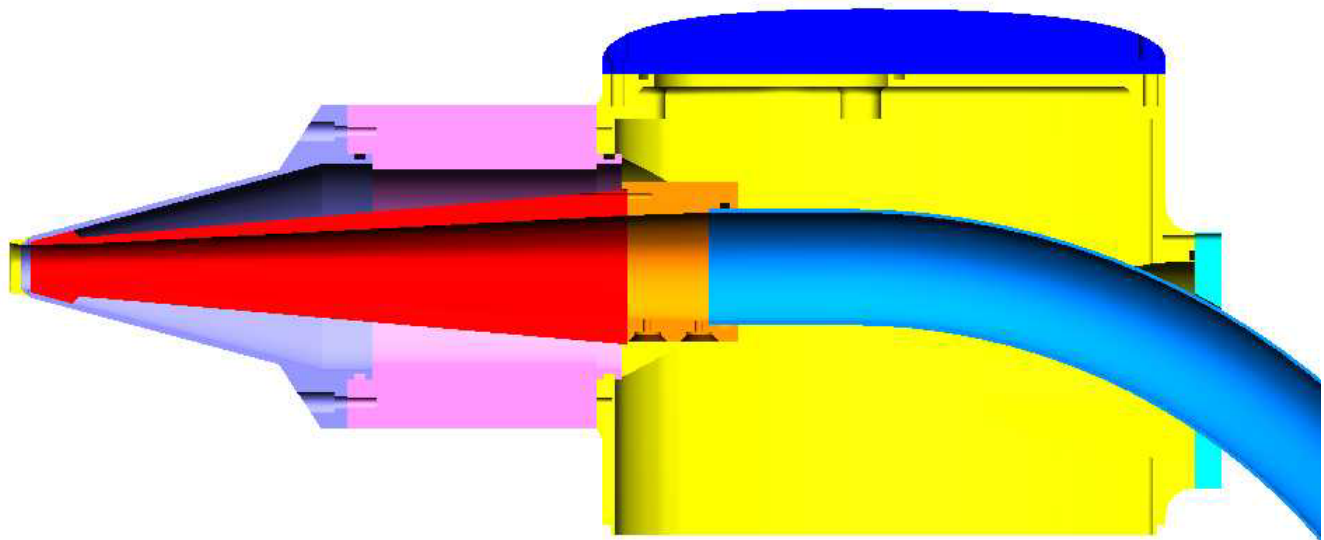


Figure S1. Detail of the LTI. Porous diffuser is red, with suction plenums above and below connected to the yellow strut plenum. Sample flow passes through the curved blue tubing to enter the fuselage (below the bottom of the figure). When in use, the hot film anemometer probe is located in the left center of the orange section. The yellow section on the inlet tip is the elliptically-curved blunt leading edge.

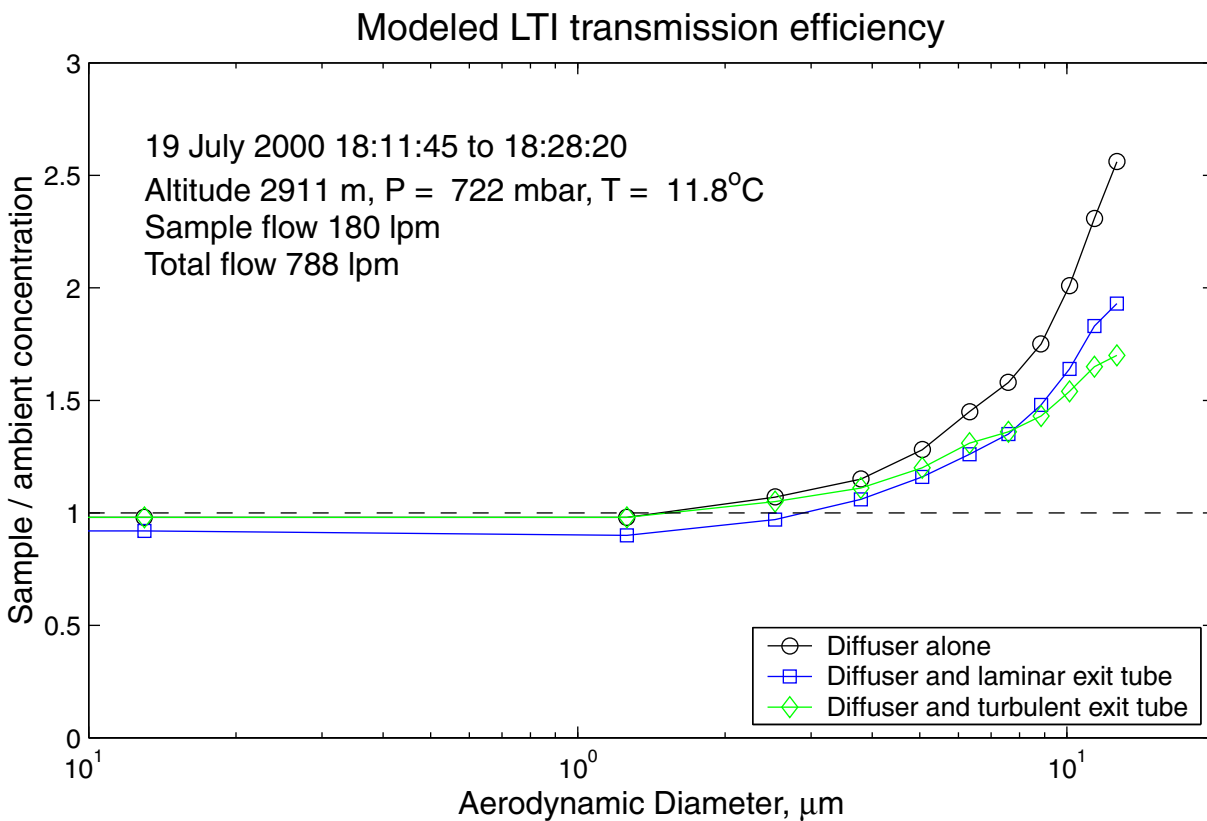


Figure S2. Fluent modeling of the enhancement in LTI sample flow due to inertial separation of particles from curving streamlines. Black circles: enhancement only. Blue squares: enhancement and losses in exit bend assuming laminar flow. Green diamonds: enhancement and losses assuming turbulent flow in exit bend. Modeling by D. Gesler.

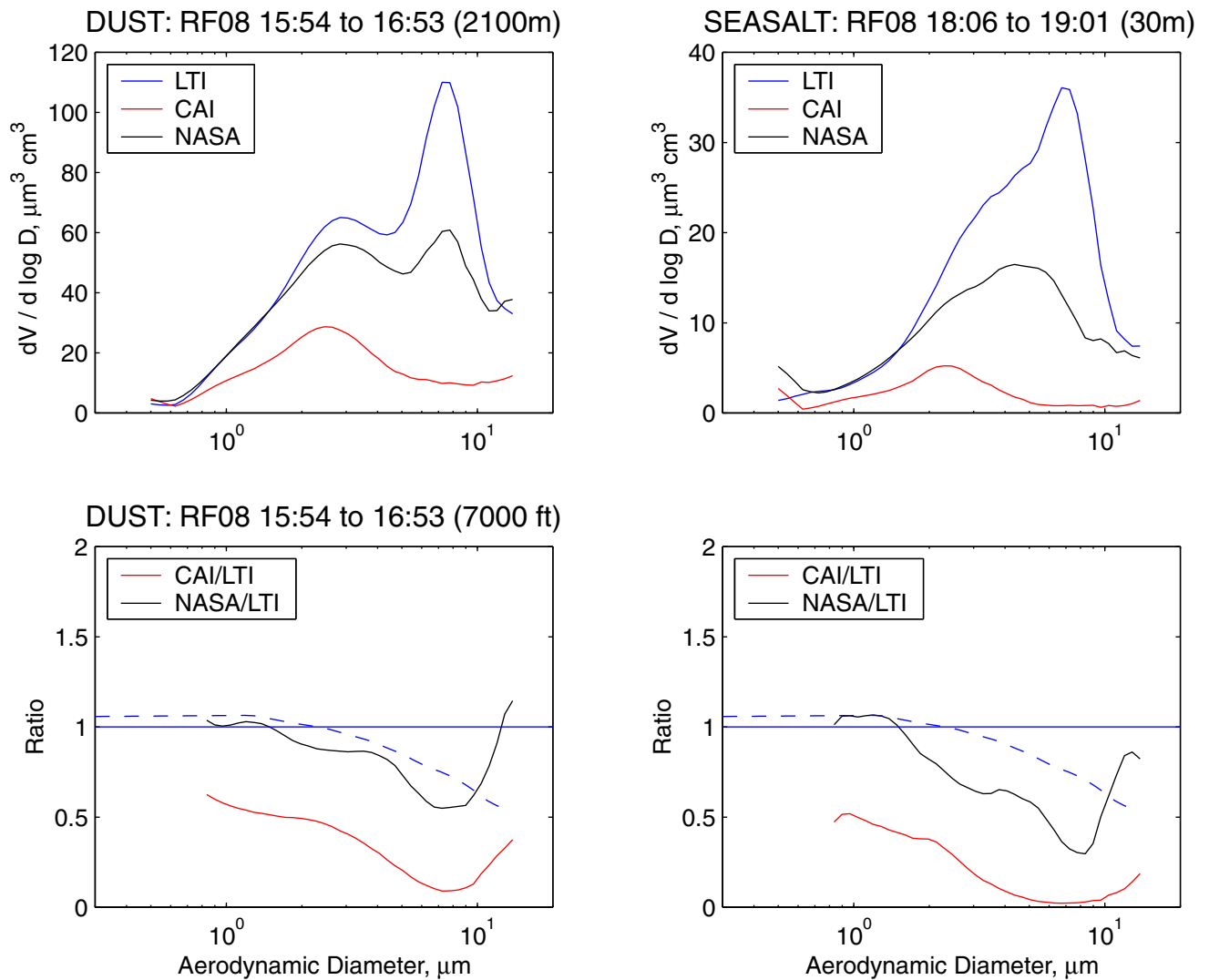


Figure S3. Typical APS data behind the three inlets. The left panels are for a flight leg in dust, while the right panels are for a MBL leg. In the top panels are volume distributions for the three inlets. As in every leg, the LTI admitted the most particles, then the SD and finally the CAI. We frequently observed two modes in the volume distribution, one peaking around 2-4 μm and the other peaking at 6-8 μm . The SD efficiency was closer to that of the LTI in dry dust legs than in the humid MBL. The lower panels show the ratios of the concentration at each size behind the other inlets to concentrations behind the LTI. The dotted lines are the reciprocal of the enhancement and loss (Fig. S2), to clarify how much of the observed differences might be due to enhancement by the LTI.

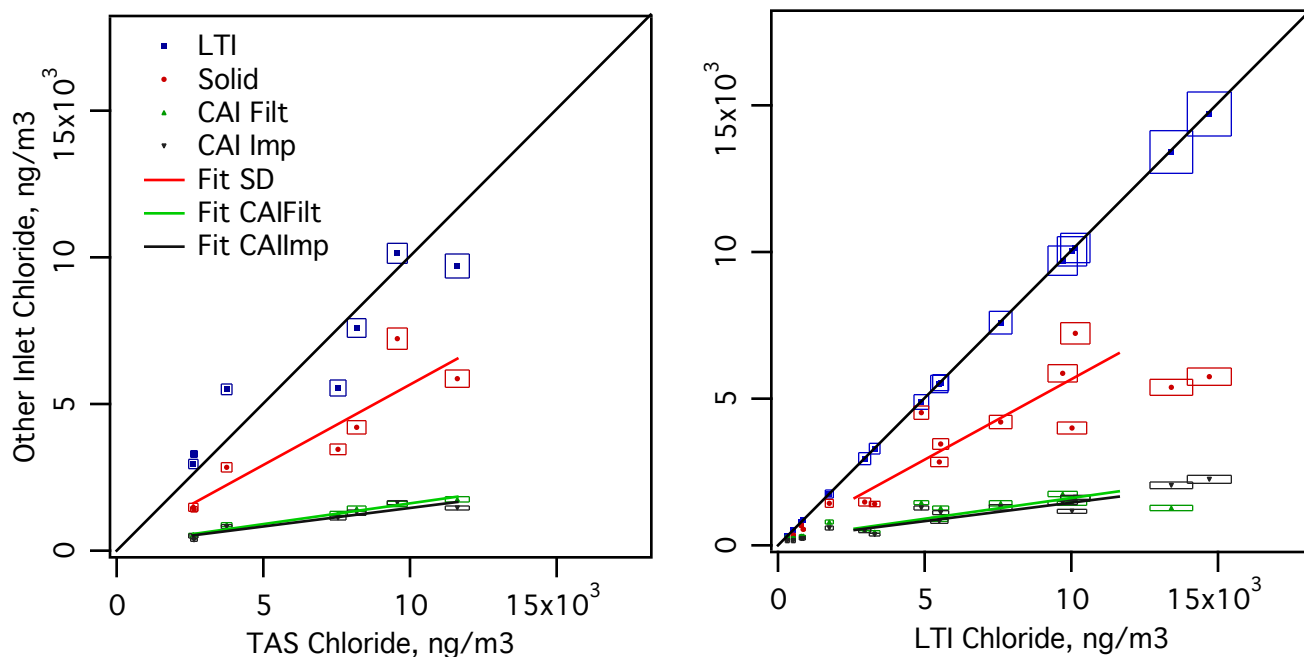


Figure S4. A comparison of chloride on filters behind the various inlets vs TAS Cl- (left panel) and LTI Cl (right). Linear fits are shown for the SD, CAI impactor, and CAI filter data. Boxes represent uncertainties derived from twice the blank variability, the detection limit, and flow uncertainty. The LTI reproduces the ambient chloride (represented by TAS) within 10-20%, while the other inlets are biased lower.

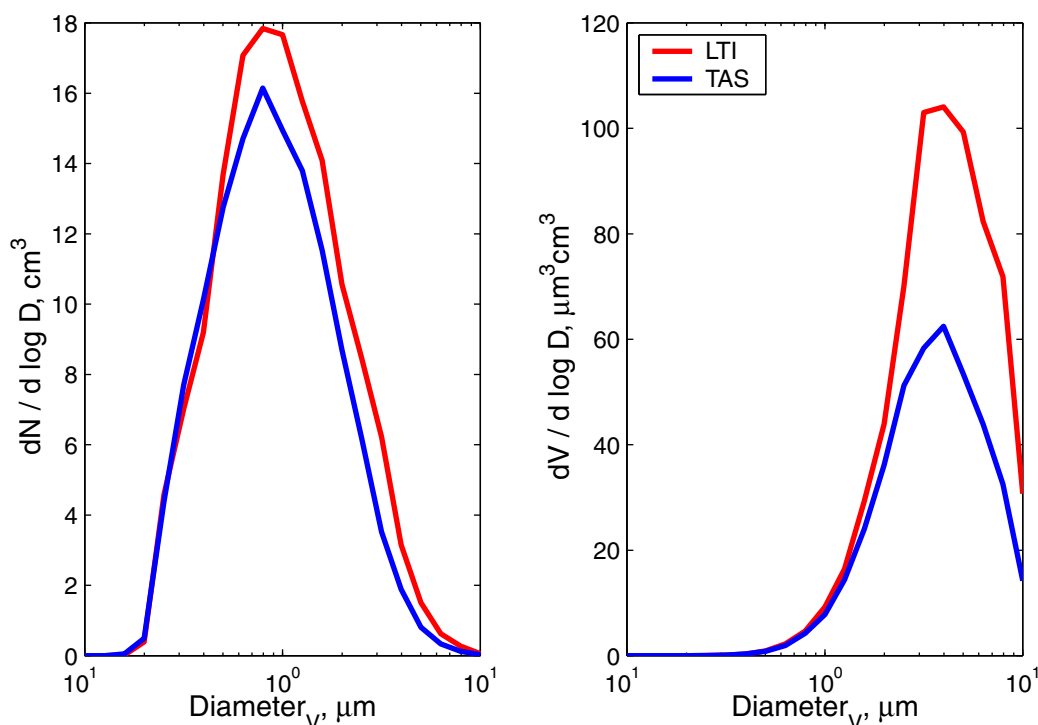


Figure S5. Comparison of SEM-derived size distributions behind the LTI and in TAS. The left panel is a number distribution, while the right is a volume distribution. The diameter was derived from an estimate of the volume of each particle. No correction has been made for the enhancement by the porous diffuser.

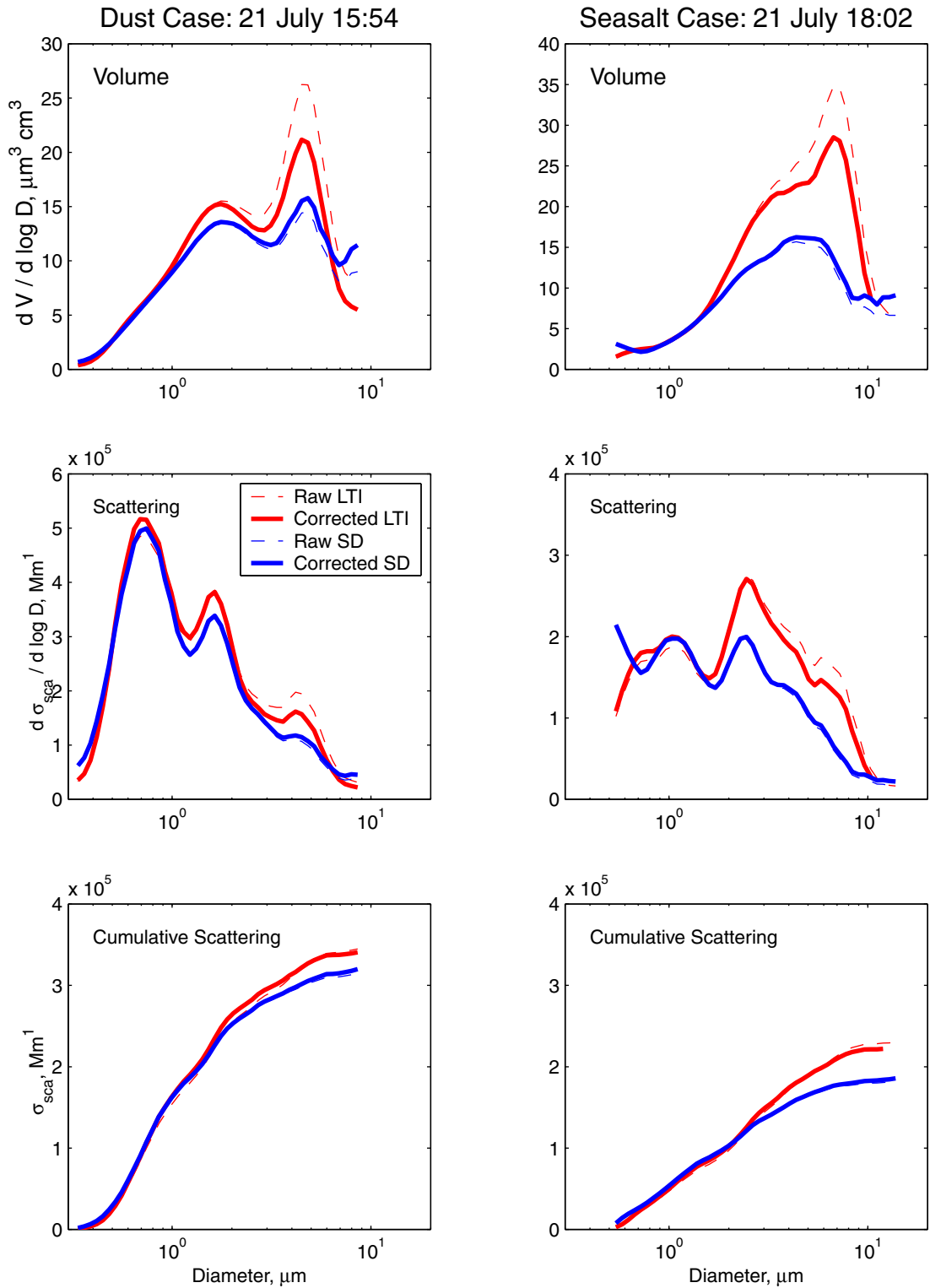


Figure S6. Accuracy of derived optical properties from the LTI and SD. The left panels are for a dry dust case, the right panels for a sea salt leg. The top panels show the best-guess corrections of both inlets for enhancement and tubing losses. The second panels use Mie theory to compute the scattering based on the size distributions and assumptions about the density and refractive indices of dust and sea salt. The bottom panels show the cumulative scattering. The leveling off at larger sizes is due to the fact that the mass scattering efficiency drops for larger particles, so they have little radiative impact.

1. Introduction

1.1 State of the Science

It has long been known that typical diffuser-and-curved-tube airborne inlet systems remove particles from sampled airstreams, so that instruments downstream receive air that has been depleted of supermicron particles. Huebert et al. (1990) noted in the Dycoms experiment that there were apparently several times more ions/m³ in stratocumulus cloudwater than in the aerosols below those clouds. This discrepancy was explained in the PASIN experiment, in which an external reference inlet was designed so that any deposits in the diffuser or tubing could be washed out and analyzed after a flight. Concentrations of soluble ions collected on Teflon filters behind five inlets with different geometries were compared with those from the reference inlet. The conclusion was that even large-diameter, gradually-curved inlet systems deplete sea salt particles by as much as 90%, although submicron particles also were depleted by tens of percent (Huebert et al. 1990).

In the PAIR program, it was further established that the losses are a strong function of aircraft speed (B. Huebert, unpublished data). A removable and extractable external sampler was used as a reference on this and several subsequent field programs. It was designed so that it could be sealed after cleaning and only opened to the airstream during sampling. Losses at 80 m/s true air speed were significant, but smaller than those at 120 m/s. A similar study by Sheridan and Norton (1998) used a bag-shaped filter inside an inlet tip as a reference to collect all particles that entered the tip. This study also found that a conventional inlet caused large losses of supermicron species, as well as significant losses of species expected to be in submicron particles.

A workshop was convened at NCAR in 1991 to assess the state of knowledge about inlet systems. The attendees concluded that it was not possible at that time to sample supermicron particles from aircraft without substantial and unquantifiable size-dependent negative biases, and made several recommendations for ways to study and improve airborne aerosol inlets (Baumgardner et al., 1991). Since most instruments require that air be decelerated to a few m/s prior to its analysis, decelerating diffusers have been widely used in airborne sampling. Apparently the highly-turbulent flow just inside the tip of these conical diffusers causes the largest particles to be impacted on the walls of the diffuser. With the possible exception of mineral particles that may bounce off the walls, this has the effect of removing large particles and distorting the particle-size spectrum behind diffusers.

As a result of these concerns, NCAR's RAF undertook the design of a common inlet to mitigate some of these problems. This Community Aerosol Inlet (CAI) incorporated several features suggested by members of the community to minimize artifacts: the CAI's tip was located forward of the nose of the C-130; all the deceleration took place in a straight line to avoid losses in high-speed bends; the diffuser angles were much less than the typical 7 degrees of many other inlets; and the flow was large enough to allow many users to sample the same air. This commonality was particularly important, since it allowed local closure experiments on aerosol properties; the aerosol spectrum would be similarly modified for all instruments that derived their air from the CAI. The CAI was used by most aerosol instruments in both ACE-1 (Bates et

al., 1998) and INDOEX. An evaluation of the CAI efficiency in the Community Aerosol Inlet Evaluation Experiment (CAINE-2) showed that the CAI worked well for submicron particles, but its efficiency dropped rapidly above that, with a 50% cut size in the 2-3 μm range (Blomquist et al., 2000).

One of the most promising suggestions from the 1991 workshop was that of University of Denver (DU) researcher Russ Seebaugh, who noted that boundary layer separation was likely in the conical diffusers used for aerosol sampling and that they could use boundary layer suction to mitigate the effects of flow separation (Seebaugh & Childs, 1970). The technique was applied to airfoil surfaces (Lachman, 1961) and aircraft air inlets. For airfoils, it actually maintains laminar flow over substantial portions of the surfaces.

From 1991 through 1999 Seebaugh and his DU colleagues Bernard G. Lafleur, Chuck Wilson, and Jungho Kim developed the concept in the laboratory with support from NSF and NOAA (Seebaugh et al., 1997). They showed that suction through holes was effective in preventing separation but did not markedly reduce turbulence intensities (RMS speed/mean speed) in conical diffusers. By using diffusers manufactured entirely from sintered porous plastic they reduced the turbulence intensity at the diffuser exits from the 50-60% range typical of solid diffusers to just a few percent (Seebaugh et al., 1996, Lafleur, 1998). The few percent residual was often not due to turbulence generated within the diffuser, but represented low frequency disturbances caused by the bulk air motion in the laboratory. Suction percentages (100 x porous diffuser flow/total entrance flow) in the range of 20% to 80% eliminated turbulence under most conditions in the laboratory.

DU researchers and Jack Fox of NCAR designed an airworthy aircraft aerosol inlet that was fabricated in the NCAR shop to meet demanding schedules for flight testing. This inlet incorporated a sintered stainless steel porous diffuser machined following recommendations of Mott Corporation. It featured a contoured leading edge which suppressed the effects of leading edge separation and made the inlet performance robust under conditions of changing attitude. Relating sampled aerosol mixing ratios to ambient values requires understanding inertial enhancements in the conical diffuser. Particles separate from streamlines and concentrate in the sample flow. Calculations were made using laminar flow equations (Gesler, 2000).

These porous diffusers are the heart of a new Low Turbulence Inlet (LTI) that we hope to use in the ACE-Asia experiment to characterize aerosols leaving Asia for the Pacific. However, before awarding flight hours for this program, NSF demanded an answer to a critical question: Does the removal of turbulence from an inlet actually improve the efficiency with which it can bring large particles into an aircraft? Flight tests of the LTI efficiency for admitting sea salt and mineral dust particles were necessary to answer that question.

1.2 PELTI

At the suggestion of Eric Saltzman, a small working group was convened to plan, execute, and assess the in-flight evaluation of the size-dependent passing efficiency of the LTI developed by the University of Denver researchers. The working group concluded that two hypotheses should be tested:

A. The LTI has a demonstrably higher aerosol sampling or transmission efficiency than both the CAI (the NCAR C-130 community aerosol inlet) and traditional solid diffusers for particles in the 1-7 μm range.

B. It is possible, using the LTI, to sample and characterize the number-size and surface area-size distributions of ambient dust and seasalt inside an aircraft with enough accuracy that uncertainties arising from inlet losses will contribute less than 20% to the assessment of radiative impacts.

Our focus is aerosol sampling and transmission efficiency, but our needs in this regard are determined by scientific questions regarding aerosol radiative forcing of climate. While it is desirable to collect all sizes of particles efficiently from an aircraft, the criterion for deciding whether ACE-Asia can meet its coarse-particle goals depends most strongly on sampling particles in the radiatively and chemically important 1-7 μm range. Thus, we will determine size-dependent sampling efficiencies in the 1-10 μm range.

The optical depth for any component of the aerosol, τ_i , depends on the integral of extinction over all radii, r . For a non-absorbing aerosol, this is a function of the mass-scattering efficiency of the substance, $\alpha_i(r)$, and the mass of the substance, $m_i(r)$, in each size interval, as well as the pathlength containing that type of material, H_i .

$$\tau_i = \int_r \alpha_i(r) m_i(r) H_i dr$$

If the airborne inlet does not pass all sizes efficiently, an efficiency term, $\epsilon(r)$, must be included with the mass to compute the apparent optical depth, τ_i' :

$$\tau_i' = \int_r \alpha_i(r) \epsilon(r) m_i(r) H_i dr$$

The error in radiative forcing due to sampling losses depends, then, on both the transmission efficiency and the fraction of the mass and total optical depth in each size interval. For those sizes that contribute little to the optical depth, a poor transmission efficiency will cause little error in radiative forcing calculations. It is worth noting, however, that undersampled sizes could still cause significant errors for other issues, such as the computation of deposition fluxes and heterogeneous reaction rates.

2. Methods

2.1 Overall approach

2.1.1. Testing Hypothesis A

Hypothesis A can be tested relatively simply, since it only requires measurements inside the aircraft, on several air streams that have already been decelerated. We used three matched aerodynamic particle sizers (TSI Model 3320 APS's) to measure the physical size distribution

behind our three test inlets: the LTI, CAI, and SD. The difference between the APS distributions provides a direct test of Hypothesis A. Nephelometers were used to compare the scattering behind each inlet and to provide a real-time signal in flight to guide the tests. They also provided a relevant integral measure of light scattering that is appropriate to the tests and one of the goals of ACE-Asia, radiative transfer.

We also collected filter samples for chemical analysis behind each of these inlets. That included both Teflon filters for ion-chromatographic analysis (IC analysis of major anions and cations by Barry Huebert's group) and streakers with Nuclepore filters (SEM analyses by Jim Anderson). In dust, Anderson counted and sized the particles behind each inlet. The SEM was set up to size particles without chemical analysis, so that it could get statistics on thousands of particles.

2.1.2 Testing Hypothesis B

Hypothesis B is considerably more difficult to test, since it involves comparing aerosol distributions behind the LTI to those in ambient air. The crux of the problem is to measure the ambient (reference) distribution with a system that does not itself suffer from inlet or other artifacts. The two devices that are the least likely to exhibit inlet losses are FSSP's and total aerosol samplers (TASs). Virtually all other samplers and OPCs (even wing-mounted ones) derive their samples from some type of inlet, whose potential for losses would compromise the tests.

The FSSP-300 seemed to offer the best hope for characterizing the ambient size distribution, even though its response depends strongly on assumptions about particle refractive index. We flew three 300s, which were set up identically and intercalibrated in the laboratory at RAF to minimize differences. Two were flown on the wings, to assess the precision possible with 300s. The third was set up behind the LTI, where the airspeeds were much lower. As long as all three were set up identically, using the same index of refraction, they should be able to identify differences caused by the LTI. Of course, if the choice of refractive index is wrong, this would cause errors in the apparent sizes at which efficiencies are calculated. In addition, the flow regimes in the sensing volumes are very different in the free ambient airstream and inside the aircraft, and this also introduces uncertainties. It is worth noting that the counting efficiency (y-axis) of 300s has rarely been calibrated, in contrast to their sizing ability (x-axis).

One of the most defensible references is the bulk concentration of particles, as measured by the TAS designed and built in the NCAR shop. This external sampler permits an analysis of every particle that enters the inlet tip, whether it has been deposited on the inside of the diffuser or collected on its filter. The diffuser is lined by removable cones, which are replaced with each filter sample and extracted after the flights. As long as we sample isokinetically, we can be assured that the sum of the cone extract and its filter contains every particle that entered the TAS tip. This was used to measure reference ambient concentrations of both seasalt and dust. When sampling dust, the size of mineral aerosol was preserved in the TAS extracts (except for aggregates of big particles and clays), so that the ambient (TAS) and LTI size distributions could both be measured directly from filters by SEM.

2.2 LTI Configuration

The PELTI inlet was an extension of the flight inlets tested in April-June 2000 on the NCAR Electra (Figure 2.2.1) developed by Bernard G. Lefleur, Russ Seebaugh, Dave Gesler, and J. C. Wilson at the University of Denver (DU). The porous diffuser for the Electra Low Turbulence Inlet (LTI) (Figure 2.2.2) was a slightly modified version of the most successful diffuser developed and tested earlier in the DU laboratory. The evolution of the LTI was very rapid prior to PELTI due to the efficient airborne testing program facilitated by the NCAR Research Aviation Facility and the design and fabrication assistance offered by Jack Fox in the NCAR shop. The design parameters for the laboratory and Electra LTIs were:

- Porous diffuser 85.3 mm long constructed as single segment.
- Diffuser entrance diameter 11.2 mm.
- Diffuser exit diameter 18.9 mm, giving an area ratio of 2.3.
- Compound internal expansion: a 4.4 mm segment at 0 degrees (straight section), then a 10.1 mm segment at 2.0 degrees (total angle), and finally the remainder of the diffuser at 6.0 degrees.
- Porosity 20 micrometers.
- Short solid entrance section upstream of the porous diffuser.
- Outer sheath created a plenum chamber for suction flow that completely surrounded the porous diffuser.

The mounting strut for the Electra LTI incorporated an access port for a hot film anemometer probe to measure the mean flow velocity and the turbulence intensity at the diffuser exit during flight. The sample flow was withdrawn through a 19.1 mm inside diameter tube attached to the diffuser exit. The limited space available on the window mounting plate required a small-radius 90-degree bend in this sample flow line immediately behind the porous diffuser. The sample line passed through the window plate to a laminar flow element (LFE) flow meter and vacuum pump. The suction flow was collected inside the strut and also passed through the window plate to a second LFE flow meter and vacuum pump. Pressures were measured at the diffuser entrance (in the solid entrance section) and at the diffuser exit.

The laboratory inlet and the first version of the Electra LTI used a porous plastic diffuser. The porous plastic material was dimensionally unstable and the pores tended to close gradually with use. There was also concern that any water ingested by the diffuser would freeze during high altitude flight and damage the diffuser. The porous plastic diffuser was replaced with a porous stainless diffuser near the end of the Electra flight program. The porous material was Mott Corporation's 20 micron grade. [Note that the micro grade is a designation internal to Mott Corporation and should not be interpreted as a pore size.]

Attempts were made to align the axis of the inlet to the average local flow direction at the inlet location on the Electra by measuring the flow direction with a flow angle probe. Because there was some flow interaction between the inlet/strut assembly and the flow angle probe, it was impossible to precisely align the inlet with the local flow. We believe, however, that the inlet was aligned within 2 degrees of the local flow direction with the inlet/strut installed at an aircraft angle of attack of 2 degrees. Excursions in aircraft angle of attack accompanying altitude

changes and fuel consumption resulted in an overall range of misalignment of about 1 to 3 degrees.

Initially, a sharp leading edge was used on the Electra LTI. However, low turbulence levels at the diffuser exit could not be achieved at isokinetic flow. It seemed likely that the flow separated just inside the sharp leading edge, inducing turbulence that could not be controlled using suction. After replacing the sharp leading edge with a blunt (elliptical) leading edge, turbulence was eliminated under most flight conditions by adjusting the suction flow. The bluntness of the leading edge was reduced by a factor of two and turbulence control was again achieved. Further reductions in leading edge bluntness resulted in a failure to reduce turbulence, so the intermediate contour was used. This elliptical contour has a leading edge whose radius is larger than the radius of the inlet throat by approximately 6.5%. Thus the leading edge of the inlet encompasses 13% more area than the throat area.

Several additional modifications to the Electra LTI were made in the design of the University of Denver LTI used in PELTI:

- The diffuser exit was increased to 25.4 mm. This was the maximum value that had consistently achieved fully laminar flow in the laboratory facility, and was also the maximum value that could be incorporated into the strut and aircraft window. This increased the area ratio of the inlet to 5.2 (Figure 2.2.3).
- A 3-segment porous diffuser was used to facilitate manufacture. No variations in aerodynamic performance were observed as a result of the 3-segment configuration.
- The longer diffuser required a longer suction flow plenum; this extended the inlet leading edge forward 61 mm.
- The axis of the PELTI inlet was aligned within 1-2 degrees of the average local flow direction at the inlet location on the C-130.

The LTI was mounted on the right side of the C-130, in the forward-most access port (Figures 2.2.4 and 2.2.5).

2.3 Location of inlets, plumbing, and layout

Since internal tubing has the potential to remove particles and mask the differences between the inlets themselves, we made every effort to design plumbing that would have minimal impact of the size distributions. A second design criterion was to make the plumbing as similar as possible between the LTI, SD, and CAI systems, so that any unavoidable tubing losses would be similar behind all the inlets. Tubing is diagrammed in Figures 2.3.1, 2.3.2, and 2.3.3.

The CAI “brewery” plumbing (Figure 2.3.4) that was used in ACE-1 and CAINE-2 was used as an example, because its passing efficiency vs size had been measured in the lab with monodisperse uranine particles (Blomquist et al., 2000). It passed particles up to 6 μm with nearly unit efficiency, and had an overall 50% cut at 7 μm . Those measurements showed that the most serious losses were in the pickoff tube from the CAI. The 2.6 m-long arch of nickel-plated 4.4 cm id copper tube had a high efficiency for particles below 10 μm at its design flowrate of 200 lpm. Thus, for the LTI we used 2.7 m of 3.8 cm id tubing, while the NASA inlet used 3.5 m

of 3.2 cm id tubing (both for nominal 100 lpm flows; Figure 2.3.5). The main delivery tubes from all the inlets had residence times of 1-2 seconds, except when the LTI flow was decreased to check for enhancement at lower flow rates (RF03:1718-1733 and RF05:1558-1610). At those low flows the residence time was around 5 sec, which could have permitted more sedimentation of the largest particles.

The longer run of tubing from the SD resulted from the fact that it was the only inlet on the left side of the aircraft. All the fuselage apertures on the right side were used, with the LTI in the highest one, TAS at shoulder-level, and the CAI pickoff tubes just above the cabin floor (Figure 2.2.5). Immediately ahead of the LTI was an air-conditioning vent, whose flow almost certainly could not reach out 30 cm from the fuselage to contaminate the flow into the LTI. Of greater concern was the CAI forward strut, whose wake propagated turbulence into the LTI when attack angles exceeded about 2 degrees. Relative to the nose, the LTI, SD, and TAS were within about a meter of the same distance back. The CAI, by contrast, admitted its air almost at the plane of the nose.

All the filter samplers and APS/streaker/neph modules were located in the second rack on the right side of the cabin (Figure 2.3.6). Each inlet had its own 90 mm filter sampler as well as a “module,” consisting of an APS, a streaker, and a nephelometer. These modules had identical flow distribution systems that drew 25 lpm of sample air from the respective inlets and distributed it to the instruments. Flow distribution plenums (Figure 2.3.7) were made of 1.9 cm id copper tees with 1.3 cm id sidearms that sent air to the APS, streaker, and nephelometer, with the excess going to either an OPC (only on the LTI) or to waste. The cabin FSSP-300 derived its flow directly from the LTI, via an 82 cm length of 3.2 cm id PVC hose (Figure 2.3.8). The dimensions of every plumbing piece upstream of the samplers has been tabulated and this spreadsheet can be made available to anyone wanting to model these flows (from huebert@soest.hawaii.edu).

The solid diffuser inlet (SD) was built by NASA for a GTE program, based on a design by Antony Clarke. It incorporates a constant-area shroud, a 4.5 degree diffuser half-angle (Figure 2.3.9), and a 3.8 cm id tube with the largest-possible radius of curvature for a 45 deg bend to bring the air into the fuselage. Details are available from tclarke@soest.hawaii.edu.

2.4 Bulk chemical analyses

Filter collections for bulk chemical analysis were performed by Steve Howell, Barry Huebert, and Tim Bertram of the University of Hawaii. Analysis of the filters was done by Liangzhong Zhuang of UH. Zefluor 90 mm Teflon filters were exposed in 5 locations during most sample legs: in TAS and behind the LTI, SD, CAI, and the 1 μm CAI impactor. A field blank (on for 10 sec) was also exposed for every sampler on each flight. The blank for each flight was subtracted from that flight’s samples, and the variability of that flight’s Teflon blanks was used to estimate the uncertainty of each value. Tedlar substrates were used in the CAI impactor to collect particles larger than 1 μm . Since only one substrate blank was exposed on each flight, the variability of the Tedlar blanks over all flights was used to estimate the uncertainty in analyte.

TAS cones were extracted by agitating for 2 minutes with 30 ml of DI water. These extracts were also sent to UH for IC analysis. Only those TAS samples with Teflon filters were extracted and analyzed by IC. TAS cones paired with Nuclepore filters were extracted with ultrasound and filtered through small Nuclepore filters for SEM analysis (section 2.5).

All Teflon filters and impaction substrates were unloaded in the field, sealed into microclean polyethylene bags, and shipped by FedEx to UH for ultrasonic extraction (1 ml of ethanol and 9 ml of DI water) and ion chromatographic analysis. The IC analysis procedures were identical to those described by Huebert et al. (1998). Above-blank analyte masses (in ng) were then divided by the volume of air drawn through each sampler to derive ng/m³ of analyte in ambient air. While each sample was analyzed for acetate, formate, methanesulfonate, chloride, nitrate, sulfate, oxalate, sodium, ammonium, potassium, magnesium, and calcium, some ions did not routinely exceed the noise defined by twice the standard deviation of the blank. Thus, most of the concentrations reported below are for chloride, sulfate, sodium, magnesium, and calcium.

We found several extremely high Na blanks during the experiment, in roughly 10% of the samples. To determine the cause we analyzed ten Zefluor 90 mm Teflon filters directly from their box and found that some had up to 10 ug of Na per filter. The fraction of contaminated filters is small enough that we failed to note it prior to using this lot for PELTI. Most of the Na data is still useable (we loaded the filters heavily with sample when we realized the blanks were variable), but the error-boxes are far greater than we would have preferred. In the future we will pre-wash all Zefluor filters, a tedious procedure that now appears to be essential for this product line.

Thus, the NSS values reported below are based on Mg rather than Na as an indicator of sea-salt sulfate. Since Mg also is likely to be present in dust, this will cause an underestimate of NSS in the dustiest samples.

2.5 SEM analyses

SEM sample collection and analysis was performed by Dr. Jim Anderson, of Arizona State University. Samples for SEM were collected using programmable “streaker” aerosol samplers (PIXE International) set up as one-stage filters and using discreet movements of the filters (rather than continuous motion, from which the streaker derives its name). Each inlet (LTI, CAI, and NASA) had an identical streaker with an electronic mass flowmeter. The streakers used a sucking orifice (1.5 x 8 mm) behind a rotating 85 mm filter stage; each sample on the stage was separated by a rotation of 9°, corresponding to about 5mm. All three streakers were operated by a single controller so that the three would simultaneously move to change samples. The streaker exposures were coordinated with the TAS and UH filters. Filters used were 90 mm Nuclepore membranes with 0.4 µm pores, the same filters used for free troposphere samples with the TAS. By using sucking orifices with no support bars, the streaker samples got uniform particle loading and therefore avoided the problems associated with typical filter holders in trying to quantitatively determine particle concentration. Support plates for Nuclepore filters in the TAS were designed to mimic the streaker orifices as much as possible in that they had a uniform pattern of 2 mm holes; SEM analysis could be done on areas over the holes, avoiding areas

above support bars through which there was no flow. Concentrations for the TAS were calculated for the effective filter area defined by the holes in the backing plate.

The instrument used for analysis was an automated JEOL 5900 SEM with a NORAN Voyager-4 image analysis system using software routines developed by J. Anderson (Anderson et al., 1996). In order to analyze the size distributions and number concentrations of many thousands of particles (a minimum of 5,000 particles per sample and up to 25,000 particles in some samples), no chemical analysis by EDS was done. However, the samples were looked at briefly by manual methods with qualitative EDS to determine the nature of the aerosol. The minimum particle size used was 0.2 μm diameter (larger than the usual 80 nm, due to use of lower magnification) and there was no maximum except the practical limit for quantifying concentrations of around 10 μm determined by the frame dimensions of 57 x 57 μm and a guard band of 4 μm . Pixel size was 56 nm. Parameters directly measured included particle area, maximum diameter, minimum diameter, and external perimeter. Derived parameters including aspect ratio, average diameter, circularity (a shape factor), and volume were calculated from these.

Because the TAS filters exhibited a systematic radial variation in particle loading, sections were cut from up to 4 locations across the radii of the TAS filters and analyzed. Particles that stuck to the sides of the TAS cone were extracted using ultrasound and high purity, filtered water and deposited on 25 mm Nuclepore membranes with 0.4 μm pores. A backing glass-fiber filter was used to ensure even particle loading. These cone extract filters were also analyzed by SEM. Because of high particle loading on the samples discussed, the blanks were negligible.

Analysis of each sample was done by setting up a grid of the 57 x 57 μm frames, typically 15 x 15 frames with 70 μm separations of their centers. This covered an area of roughly 1 x 1 mm, which fit within the areas of uniform loading for both the streaker and TAS. The analysis was then allowed to run until either a minimum number of particles was found or, on overnight runs, for the entire grid.

Most of the SEM data discussed below has not been processed other than to calculate the “average diameter” (the average of the minimum and maximum diameters) or a few other derived parameters. The concentration data are binned either by average diameter or by a diameter derived from the area.

2.6 Aerodynamic particle size measurements

Aerodynamic Particle Sizers (APS, Model 3320, TSI Inc, St. Paul MN) (Wilson and Liu, 1980) were used to count and size particles according to their aerodynamic diameter, D_{ae} , in the range from 0.8 to 13 μm downstream of each of the three inlets, the LTI, CAI, and SD. The units were operated at the standard manufacturer's flow rates of 5.0 l/min total, 4.0 l/min sheath and 1.0 l/min sample volumetric flow. APS control and data acquisition was done via computer and digital communication which operated the three systems in parallel on a 5 minute, interruptible sample cycle. The data were displayed in real time and stored for subsequent plotting and analysis. Each APS unit drew its 5 l/min from a distribution plenum on each inlet, as described above. The APS measurements were overseen by Steve Howell of UH and Dave Covert, of the University of Washington.

Before and after the PELTI flights, the size calibration of the three APS units was checked using monodisperse polystyrene latex spheres in the range 1 to 3 μm at the RAF facility. The relative counting efficiency of the APS units was determined as a part of the size calibration tests with monodisperse aerosol. Before flight 7 the APSs were also calibrated in the field, using both latex spheres and glass beads as large as 8 μm .

The flow calibration and sizing of the APS was tested as a function of pressure from 840 to 600 mb prior to the flights. Volumetric total and sheath flows were maintained at the nominal values $\pm 2\%$ over the range of pressures tested by the APS flow measurement and feedback circuitry. The 1 l/m sample flow, determined by the difference between the total and sheath flows, was maintained to better than $\pm 2\%$ since the total and sheath flows drifted proportionally as pressure changed. For 1 μm latex spheres the indicated size decreased by 3% when the pressure was decreased from 820 to 600 mb which is consistent with previous studies of the pressure effect on sizing (Rader et al., 1990).

For at least one interval during each flight, the inlet configuration of the three APS units was reordered by switching Y-pattern ball valves such that all instruments sampled in common from the CAI inlet. This was then used as a reference measurement to which measurements and differences observed when sampling from the individual inlets could be compared. Two of the APSs usually were in good agreement, but the third (usually behind SD) diverged enough that we include a corrected version of its data in many plots.

2.7 FSSP-300 observations

One approach to evaluate the passing efficiency of the LTI was to measure aerosol size distributions with two FSSP-300 optical spectrometers. One FSSP was mounted on the left wing pod and the other was located inside the cabin, behind the LTI. The FSSP-300 measures the light scattered from individual particles that pass through a focused laser beam (0.6328 μm wavelength). This light level is converted to a particle size using Mie scattering theory accompanied by the assumptions that the particles are spherical with a known refractive index (Baumgardner et al., 1992) and that the Mie function is single-valued for each light level. The concentration of particles is determined by dividing the total number of particles in each size category by the volume of air passing through the probe during a specific period of time.

Two FSSP-300s were provided by the NCAR Research Aviation Facility and NASA Ames Research Center. Darrel Baumgardner and Jeff Stith oversaw these measurements. A third 300, from the University of Hawaii, was not included in this analysis due to instrumental difficulties. Prior to mounting on the aircraft, the probes were calibrated with spherical polystyrene latex beads (refractive index = 1.58) and crown glass beads (refractive index = 1.51) over the entire size range of the probes (nominally 0.3 – 20 μm at a refractive index of 1.58). The gains of the amplification sections of both probes were adjusted to insure that each probe showed peaks in identical channels for the different calibration sizes. There is approximately a 20% uncertainty in determining the size of particles from the FSSP scattered light measurements. The source of this uncertainty is primarily from non-uniform laser light intensity, uncertainty in light collection angles, and unknown refractive index. As we are assuming that both probes are measuring the

same type of particles, the uncertainty in refractive index may cause sizing errors, but will not contribute to any differences that might be observed between the size distributions measured by the cabin and wing-mounted probes. Small differences in collection angles will make a small contribution to sizing differences and the Gaussian intensity distribution of the laser beam may cause differences, although the average uncertainty should be similar for the two instruments.

The sample area of the FSSP-300 depends upon the size of the optical mask that selects the center of the laser beam, the preciseness of the optical alignment, and the ratio in gains between the two detectors that define this optical sample volume. Care was taken to align the two probes as well as possible, but there is at least a 20% uncertainty in the sample area assumed for the two probes. The sample volume is the product of the sample area, the particle velocity, and the sample period. The particle velocity of the pod-mounted probe is assumed to be the ambient air speed of the aircraft. This could be in error by as much as 10%, as we don't know what effect the mounting location has on the airflow. Modeling indicates that the airflow at the probe location should be near free-stream, but this has yet to be verified. The cabin-mounted probe was installed in a pressure sealed vessel and a special insert in the probe sample inlet took the air from one of the LTI exhaust ports and directed it through the laser beam. Another insert, connected to a vacuum source, was located directly behind the laser beam and with an exit tube the same diameter as the inlet tube (5.5 mm diameter) so that very little pressure drop would occur between the inlet and exit. The particle velocity is calculated from the flowrate, recorded on the data system, divided by the cross-sectional area of the tube ($23.8 \times 10^{-6} \text{ m}^2$). All potential sources of leaks in the probe sampling head were sealed to insure that the measured flowrate was a true representation of the particle flow through the probe. The expected uncertainty in particle velocity is on the order of 10%, primarily because of the possible deceleration of particles in the gap between inlet and exit tubes of the insert.

The expected error in determining concentration, using propagation of errors and assuming uncertainties of 20% and 10% in sample area and particle velocities, respectively, is approximately 22%. The particle volume, determined by summing the individual sample volumes, will have an uncertainty of approximately 40%. However, it is important to note that we do not know the exact nature of the flow through the sample volume of the cabin FSSP. It may be plug flow (in which case the flowrate computation above is fine) or it may be much more complex, involving eddies and turbulence that would invalidate the simple velocity calculation. The lack of any calibrations of concentration measurements makes it impossible for us to put realistic error-bounds on concentrations from the cabin FSSP.

2.8 Nephelometers

Three identical Radiance Research single-wavelength nephelometers were used to continuously measure total light scattering behind each inlet. A fourth was configured to measure only submicron scattering behind the LTI. These generated a continuous record of light scattering to compare with size distributions and chemical concentrations. Each neph drew 10 lpm from its distribution plenum.

3. Results

3.1 Flight operations

To gain access to both sea salt and mineral dust aerosols, the PELTI experiment was flown out of the St. Croix airport (STX) in the US Virgin Islands. We ferried from Colorado to Miami International Airport on 5 July (FF01), then proceeded to STX on 6 July (RF01). We remained in STX until 22 July, when we ferried back to Miami (RF09 or 10) and then to Colorado on 23 July (FF02). Although our stay in STX coincided with a minimum in dust concentrations between two very large events, we encountered adequate dust and sea salt to test the LTI properly. Table 3.1.1 lists the conditions of each flight leg. Flows are considered to be isokinetic if the velocity at the leading edge of the inlet is equal to the free stream velocity. In this condition, the throat velocity exceeds the free stream velocity by approximately 13%. Flight reports from all PELTI flights can be found on the ACE-Asia web site, saga.pmel.noaa.gov/aceasia/.

Table 3.1.1 PELTI Flight Legs. APS ON and APS OFF are the times the APS averages began and ended. The APS times commonly differ by a few minutes from the filter sampling intervals. LTI % Suction is the fraction of total tip flow that is removed through the porous diffuser.

RF #	Leg #	APS ON CUT	APS OFF CUT	Alt. m	LTI State	LTI % Isokin	LTI % Suction	Filter Exposure? TAS-Tef/ Nuc.
3	1	17:18	17:33	60	Lam	97	94	N
3	2	17:37	17:50	60	Lam	95	90	N
3	3	17:57	18:07	60	Lam	95	87	N
3	4	18:16	18:26	60	Trans.	96	78	N
3	5	18:35	19:05	60	Lam	89	91	Y
3	6	19:23	19:33	60	Turb	96	74	N
3	7	19:47	20:22	60	Lam	78	90	Y
3	8	20:39	20:49	60	Lam	111	86	N
3	9	20:55	21:20	60	Turb	93	72	Y
3	Com	21:22	21:32	60	na	na	na	N
4	1	16:46	17:34	30	Lam	93	83	Y - Teflon
4	2	17:50	18:37	900	Lam	92	81	Y - Teflon
4	3	18:47	19:46	90	Lam	96	83	Y - Teflon
4	4	19:55	20:54	2000	Lam	84	78	Y - Nucl
4	Com	20:56	21:11	2000	na	na	na	N
5	1	15:58	16:10	300	Lam	94	97	N
5	2	16:21	16:44	300	Lam	97	85	Y
5	3	16:54	17:21	300	Turb	102	60	Y
5	4	17:30	17:42	300	Lam	60	78	N
5	5	17:47	17:57	300	lam	108	87	N
5,6	Com	22:25	22:30	2300	na	na	na	N
7	1	15:36	16:20	30	Lam	103	85	Y - Teflon
7	2	16:28	17:20	30	Turb	103	72	Y - Teflon

7	3	17:44	18:43	2700	Lam	86	77	Y - Nucl
7	4	18:57	19:39	230	Lam	96	81	Y - Teflon
7	Com	19:40	19:54	230?	na	na	na	N
8	1	14:44	15:42	4100- 2270	Lam	85	77	Y - Nucl
8	2	15:54	16:53	2120	Lam	99	79	Y - Nucl
8	3	17:12	17:53	2570	Lam	96	79	Y - Nucl
8	4	18:02	19:01	30	Lam	106	84	Y - Teflon
8	Com	19:04	19:31	30	na	na	na	N

As is typical in many field programs, the first few flights involve the shakedown and resolution of instrument problems. As an example, the TAS was not fully operational until RF04. During RF03 on 11 July we used many short periods at 30 m in the MBL to test the LTI performance under a variety of conditions: laminar, turbulent, isokinetic, subisokinetic, and superisokinetic. Unfortunately, the APS behind SD malfunctioned on this flight. We flew similar legs on RF05, exploring many different LTI settings. RF05 also included flight legs over the lidar at Roosevelt Roads in Puerto Rico that was a part of the PRIDE experiment. (This was a relatively low-dust day.) After a stop in Puerto Rico to confer with the PRIDE investigators, the short ferry back to STX was labeled RF06.

RF04 was directed at the gradient of sea salt with altitude, and consisted of four hour-long legs at different altitudes. One of those was in the free troposphere (FT) at 2000 m. RF07 was similar, while RF08 included three hour-long FT legs and one MBL leg. The flights were generally flown to the east of STX, to avoid the inhomogeneity that would be caused by the wakes of other Antilles islands. We still did have to contend with variability during our constant-altitude legs, however, as a result of rain showers and the sloping of FT aerosol layers.

On a typical flight we would begin with a sounding to 2400 m to assess layering, then descend to our first sampling altitude. Once the airspeed and altitude were stabilized, the LTI flows would first be adjusted to isokinetic and laminar (on most legs). Then we would start the APS computer (it averaged the three APS outputs over every 5 minutes of each leg) and begin filter sampling. Because of the large number of samplers, it commonly took several minutes to get all the filter flows adjusted so that the other inlets and TAS were isokinetic. The RAF data system was programmed to read our flowmeters and other flight parameters, so it could display the fraction of isokinetic for all but the LTI. The LTI flows were recorded and displayed on a separate DU computer system.

On the early research flights (1 and 2) we did not have all of our equipment running properly. On flight 9 we quickly ran out of dust and flew in very low aerosol concentrations much of the time. Accordingly, most of the data analysis below is focused on flights 3, 4, 5, 7, and 8. Plots of altitude, RH, LTI fraction of isokinetic, LTI sample flow, filter exposure times, and an LTI laminar flag (2=laminar, 1=transitional, 0=turbulent) can be found in Figures 3.1.1 – 3.1.6.

3.2 LTI Aerodynamic Performance

The NCAR Electra LTI flight program (April to June, 2000) and the PELTI deployment (July 5th to 23rd, 2000) were instrumental in validating the aerodynamic behavior of the LTI developed at DU. The Electra program (1) confirmed that the diffuser internal aerodynamics were the same airborne as they were in the laboratory and (2) provided an opportunity to test and evaluate the LTI aerodynamics under non-isoaxial and non-isokinetic flow conditions. The latter could not be simulated in the laboratory. The PELTI mission tested the diffuser's performance at sea level and over extended use in a typical scientific setting. These flight programs validated the results obtained at DU's diffuser testing facility.

The LTI's aerodynamic performance was evaluated by measuring the turbulence intensity of the flow at the diffuser exit using a hot film anemometer (Lafleur, 1998). Extensive laboratory testing demonstrated that if the flow very close to the wall at the diffuser exit was low-turbulence then the entire diffuser flow was also low-turbulence. Further laboratory tests also showed that the velocity sensor could be recessed into the access port in the diffuser wall (out of the flow) and continue to quantitatively detect turbulent flow. This allowed continual monitoring of the diffuser flow while protecting the hot film anemometer and avoiding a flow obstruction.

A direct comparison of the turbulence intensity for identical flow conditions between the laboratory and in flight was not possible. Diffuser profiles could not be acquired during PELTI using identical operating parameters to those in the laboratory. However, the transition from turbulent to low-turbulence flow was repeatable and consistent with laboratory measurements for similar static pressures and airspeeds at the diffuser entrance.

Distinctions between turbulent and low-turbulence flow both in the laboratory and in the flight were unmistakable. Figure 3.2.1 shows an instantaneous velocity trace recorded in a laboratory simulation of the LTI. The dramatic transition from turbulent to low-turbulence flow is evident. The probe is located near the wall at a position of $r/r_o = 0.90$. The left side has turbulent flow with an intensity of 29% when no suction is performed, and the right side has turbulent-free flow with an intensity of 0.4% when the suction is suddenly turned on. Note that in the laboratory configuration for the time period covered by the figure, the volume flow rate at the velocity sensor remained constant while the amount of suction changed.

A similar comparison performed in-flight on the PELTI LTI is shown in Figure 3.2.2 where 47% and 4% intensities for the turbulent and low-turbulence flow, respectively, are shown. Both measurements were performed at $r/r_o = 0.90$. Note that in the aircraft configuration, both the sample and suction flows had to be varied to transition between turbulent and low-turbulence flows. The flow split between sample and suction flows that produces laminar flow in the diffuser depends on operating conditions such as pressure and total flow. Although the flow split which produced laminar flow in the aircraft differed from that seen in the laboratory, the trends in the required flow split with operating conditions were consistent between the aircraft and laboratory observations.

Lower turbulence levels were measured in the laboratory than in flight for two reasons. The vibration of the aircraft induced a vibration in the velocity sensor's mounting shaft. This

vibration of the sensor results in a velocity signal as the probe moves relative to the air. Also, the TSI Constant Temperature Anemometer (CTA) used on the aircraft had higher levels of electronic noise in the output signal that did the CTA used in the laboratory.

The LTI diffuser performance at altitudes lower than Denver was studied in the PELTI deployment. Increased air density increases the difficulty in maintaining low-turbulence flow in a diffuser. The ratio of suction flow to total flow was increased to maintain laminar flow as operating pressure increased (Lafleur, 1998). Both altitude simulations in the DU test facility and high altitude tests during the Electra program indicated that higher altitude (i.e., reduced ambient pressure) permitted higher sample line flow rate while maintaining laminar flow. At the lower altitudes achieved during the PELTI mission the maximum sample line flow rate with laminar flow decreased as expected (Table 3.2.1).

Table 3.2.1. LTI sample line flow rate as a function of aircraft pressure altitude where low-turbulence flow at the diffuser exit was observed.

Pressure Altitude	Sample Flow Rate
5330 m (17,500')	270 lpm
2290 m (7,500')	220 lpm
2590 m (8,500')*	205 lpm*
915 m (3,000')	150 lpm
60 m (200')	130 lpm

* Laboratory measurements: accelerating air to aircraft speeds produces a simulated altitude of approximately 2590 m.

The flow rates in Table 3.2.1 should be identified as “worse-case” rather than limits for ACE-Asia. Both the Electra and PELTI programs have shown that the diffuser performance at the DU facility does translate from the laboratory to the aircraft at the same pressure altitude. We believe that the diffusers that have currently flown represent the first step in optimizing the distribution of suction along the axis of the diffuser. Further optimization in the laboratory should produce higher ratios of sample flow rate to total inlet flow rate.

Super/sub isokinetic conditions could not be achieved in the laboratory test facility. Deviations from isokinetic conditions during the flight programs did not affect the ability of the LTI to reduce turbulence.

The inlet location on the C-130 (Figure 2.2.5) was directly behind one of the CAI mounting struts. The strut produced a wake that made turbulence control by suction impossible when the wake impinged on the inlet. The interference was a function of the angle of attack of the aircraft. By increasing the research speed to 220 kts IAS in the MBL, the aircraft flattened out enough that its angle of attack caused the strut wake to miss the LTI. In future programs the CAI will not be on the plane, so that the usual 200 kts IAS research speed can be used.

Laboratory tests were performed on the PELTI diffuser both before and after the deployment to evaluate the effects of extended use. The time-mean velocity and turbulence intensity as a function of both radial position and percent suction flow were the same for both pre and post

deployment tests. A 5% increase in pressure drop across the porous material at a given flowrate was measured at the front of the diffuser while an 8% increase was measured at the rear.

The manufacturer of the porous material, the Mott Corporation, has devised a methodology for evaluating the pore blockage and for cleaning the porous material. DU, with Mott's help, is adapting this methodology for maintaining diffusers used for aerosol sampling from aircraft.

3.3 Bulk filter data

The Total Aerosol Sampler was used as a reference for ambient concentrations of anions and cations. During MBL legs we put Teflon filters in TAS and ran IC analyses on the resulting TAS filters and deposits, which are compared below with filters (and one impaction substrate) behind the other inlets. Mg was used to subtract out sea salt sulfate in the computation of non-sea salt sulfate, NSS(Mg), because of unusually large variability in the Na blanks.

Average Ratios of Species Concentrations Behind Various Inlets to TAS Concentrations

Ratio	Cl	SO4	Na	Mg	Ca	NSS(Mg)
LTI/TAS	1.15	1.03	0.94	0.86	1.03	1.23
Solid/TAS	0.58	0.84	0.54	0.51	0.74	1.32
CFilt/TAS	0.17	0.52	0.20	0.19	0.25	0.86
CImp/TAS	0.16	0.50	0.18	0.19	0.24	0.79

It is evident that most species have virtually identical average concentrations $\pm 15\%$ in the TAS and behind the LTI. That suggests that the LTI is properly representing ambient bulk concentrations for these ambient mass size distributions and that the mass above about $5 \mu\text{m}$ where the LTI enhancement factor becomes large is a relatively small fraction of the total mass (see Fluent and APS results). This is consistent with the SEM volume weighted results in section 3.4. The ratios to TAS then decrease (as we would expect from APS data in section 3.5) from the SD to the CAI filter and CAI impactor. Most of these species (Cl, Na, Mg, and Ca) can be expected to exist primarily in supermicron particles, derived from sea salt or dust. However, NSS is in many cases primarily submicron, so it is not surprising that its efficiency relative to TAS is the largest for the inlets that have been shown to discriminate against large particles. In virtually all the CAI impactor samples, more than 90% of the NSS(Mg) was submicron. Unfortunately, we did not have an impactor behind the CAI.

The NSS(Mg) is an interesting case. Even when we sampled in the MBL we were in the presence of Saharan dust, which (based on our FT dust samples) contains some Mg salts. Dust-derived Mg will bias NSS(Mg) low. If only a few dust-derived large particles (ca. $> 5 \mu\text{m}$ diameter) containing Mg were collected by TAS (but similar ones could not pass through the tubing to the other samplers), that would artificially lower the NSS(Mg) in TAS relative to the actual NSS. That could very well explain the X/TAS ratios above 1 for NSS(Mg).

There were 7 flight legs with simultaneous Teflon-TAS and other filter samples. Figures 3.3.1 to 3.3.6 show concentrations relative to TAS for (respectively) Cl^- , SO_4^{2-} , Na^+ , Mg^{++} , Ca^{++} , and

NSS(Mg). The figures for Cl^- and Mg^{++} most clearly show the relationship between TAS and the LTI, because their relative error-bars are smallest: within the uncertainty defined by the scatter, the average analyte found behind the LTI is the same as that in TAS, the ambient air reference. Although the other species have larger error-bars, the table above shows that their average behavior is similar. All other inlets fared less well relative to the ambient concentrations as measured by TAS.

In the lower panels of these same figures are plots of 15 samples in which the LTI could be compared with the three other inlets. The LTI figures also have linear fits to the data of each other inlet. The LTI data is presented on the 1:1 line to illustrate the uncertainty ranges of the LTI data. It is clear from comparing the top and bottom panels that the LTI is a better reference, since the extraction of the TAS cone and filter contribute additional randomness to TAS data, relative to the single filter extraction for the LTI. TAS has a defensible physical principle behind it (it should be unbiased), but the realities of handling and extracting the cones in the field make it hard to get high precision from it.

Turbulent/Laminar samples:

To assess the impact of turbulence on the LTI efficiency, the LTI was intentionally run in a moderately-turbulent mode on three MBL legs. Only one of these had valid TAS samples on both the turbulent leg and a companion laminar leg flown immediately before the turbulent leg. The results from that one pair of samples is shown in Figure 3.3.7. The y-axis is the efficiency relative to TAS of the LTI when turbulent, while the x-axis is the same ratio when the LTI was laminar. We see that for all but Mg, the LTI efficiency was notably higher when it was laminar. The difference in the tendency to bounce between mineral Mg and seasalt Mg particles might play a role here.

However, the normal uncertainty of these samples keeps this one pair of samples from being conclusive. We thus used SD as an item for comparison, because it was operated in the same manner, regardless of whether the LTI was turbulent or laminar. Since the SD is less efficient than the LTI, the LTI/SD ratios are all greater than 1. The average LTI/SD ratios for turbulent and laminar legs are plotted in figure 3.3.8. Again, it is clear that the LTI is more efficient when laminar than turbulent, except for sulfate, whose large submicron fraction may explain its similar efficiency relative to SD.

It should be noted that the degree of turbulence in these legs was far less than that in solid diffusers. We simply increased the sample flow until the traces were not clearly laminar (often about 200 lpm in the MBL, as compared to the laminar flow of 120 lpm). At these times, however, the turbulence was a far cry from the extreme levels noticed when (for instance) a sharp leading edge was used on the LTI during Electra test flights. These paired legs should not, therefore, be used as an indication of what to expect from other solid diffusers. As we noted, the LTI/SD ratios were all significantly greater than 1.

3.4 SEM data

3.4.1 Overview

While we flew dust legs on several flights, this single-particle analysis will focus primarily on two legs from RF08 (RF08-1444 and RF08-1553). Samples from the LTI streaker, CAI streaker, SD streaker, two places on the RF08-1444 TAS filter (center and outer third), four equally spaced places on the RF08-1553 TAS filter, and the TAS cone extract have been analyzed. The LTI and CAI streaker samples were also analyzed for RF08-1712. Samples from the other two dust legs and several of the MBL sea salt legs have been examined with SEM and some analyzed quantitatively.

3.4.2 Qualitative observations

The free troposphere dust samples consist primarily of the mineral species typically associated with North African dust: quartz, clays, micas, feldspars, and a variety of minor species. In the supermicron size range aggregates of mineral particles are common, often with very irregular shapes (Figure 3.4.1). Overall the shape factors for these particles are higher (more complex shapes) than for typical Arizona desert dust. Also present in relatively minor concentrations are spherical flyash particles (indicative of coal combustion) and scattered super- and submicron carbonaceous particles (probably soot). Running these samples using chemical analysis by EDS would be necessary to derive quantitative concentrations of the anthropogenic species.

Many of the supermicron aggregates are aggregates of clays. Some of these clay aggregates are roughly spherical and others are more irregular in shape. These aggregates do not pose problems for the analysis of filter samples, but they potentially do for the TAS cone extracts. The ultrasonic extraction could have disaggregated the clay aggregates (or other aggregates, for that matter). This issue is discussed below.

The MBL samples examined show evidence of water droplets impacting on the face of the LTI streaker filters along with varying external mixtures of sea salt and mineral dust. The presence of residues from shattered water droplets makes the quantitative analysis of these samples difficult. On future use of the LTI in the MBL, the particles need to be dried before collection.

One other qualitative observation is of interest. We did a ground comparison of TAS and a streaker at ASU before PELTI. The (super-isokinetic) TAS produced clearly discernable particle distribution patterns on the Nuclepore filters. Such patterns from turbulence were not observed in the TAS samples from the C-130 during PELTI.

3.4.3 Quantitative results.

The size parameter used in the following discussion is the average diameter, calculated from the measured minimum and maximum diameters. In some plots we also compare with an effective diameter and volume computed from each particle's area times its smallest dimension. Concentrations are reported as particles per cubic centimeter.

TAS filters and extracts. The TAS samples are assumed to represent the ambient aerosol, but measuring that ambient aerosol is not without complications. The distribution of particles on the filters varies radially, with lower concentrations on the outer portions. However, the maximum variation in number concentration across the filter is at most 12%. The TAS filter with the greatest radial variation, RF08T1553, was analyzed at four distances from the center; the results are shown in Table 3.4.1. The concentration of particles in the cone was added to a weighted average of the four filter sections and the result is used for comparison with the LTI and CAI. The averaged values are very similar to those for section M, so for sample RF08T1444 (which has less radial variation) the values for the middle section are used.

Table 3.4.1. TAS sample RF08T1553. Four sections of the filter were analyzed: middle (M), annulus 10-20 mm (A), annulus 20-30 mm (B), and annulus 30-40 mm (O). Weighted average is based on the area of each section. Number concentrations in particles/cm³; volume concentrations in $\mu\text{m}^3/\text{cm}^3$. A total of 55,270 particles were analyzed.

RF08T1553		Filt M	Filt A	Filt B	Filt O	Wtd.Avg	Cone	Wtd.Av + Cone
D _{AV} = 0.3 - 0.79	Num	5.27	5.15	4.84	4.90	4.95	0.31	5.26
	Vol	0.68	0.62	0.59	0.58	0.60	0.03	0.63
D _{AV} = 0.8 – 1.99	Num	5.30	5.03	4.50	4.37	4.59	0.25	4.84
	Vol	7.55	7.12	6.16	5.93	6.32	0.32	6.64
D _{AV} = 2.0 – 3.99	Num	1.46	1.52	1.30	1.17	1.29	0.08	1.37
	Vol	14.36	15.13	12.76	11.55	12.77	0.87	13.64
D _{AV} = 4.0 – 8.0	Num	0.27	0.32	0.25	0.22	0.25	0.02	0.27
	Vol	11.85	13.68	11.87	10.75	11.72	1.21	12.93
Total	Num	13.08	12.82	11.69	11.45	11.88	0.75	12.63
	Vol	38.06	44.75	36.40	33.66	36.86	3.11	39.97

In order to evaluate whether significant numbers of aggregate particles were present on the TAS cone but disaggregated during extraction, a comparison can be made of the total number of particles and volume concentrations on the cones relative to those on the filters. Volume is conservative and would not be altered by extraction unless there were considerable soluble material in the aerosol. The qualitative examination of the TAS filter sections did not reveal any substantial amount of sea salt, sulfate, or other possible soluble species. The loading on the cone extract for RF08T1444 was 7.24×10^6 total particles, versus a loading on the filter between 79.8×10^6 (TAS filter center) and 71.6×10^6 total particles (outer part of TAS filter). (These are numbers that are independent of airflow.) The cone has roughly 10% of the number loading on the filter. The mean single particle volume (from direct measurement of particle area and its smallest diameter) for the cone extract is $2.83 \mu\text{m}^3$ versus a mean volume on the filter of between $3.70 \mu\text{m}^3$ (filter center) and $2.63 \mu\text{m}^3$ (outer part). Two conclusions can be reached by this comparison and also from Table 3.4.1: (1) large particles have a greater radial variation than small particles, and (2) the TAS cone did not have a substantially enhanced concentration of larger particles relative to the filter.

LTI streaker results. The streaker samples have uniform particle loading, so the calculation of concentrations and size distributions is straightforward. The only problem with the LTI samples is that the calibration of the mass flowmeter used changed by 12 % between calibrations before and after PELTI (the same flowmeter had survived 7 weeks of INDOEX with no changes - the

problem in PELTI may be due to repeated exposure to wet sea salt). The calibration at the end of PELTI is used, but the concentrations calculated using the first calibration are also presented for comparison.

The number concentration for RF08LS1444 is 15.46 particles/cc [13.64 if the earlier calibration is used] and that for RF08LS1553 is 14.82 [13.08]. These compare quite well with the total concentrations from the TAS filters.

CAI streaker results. The CAI streaker samples consistently have lower particle concentrations than the LTI streaker or the TAS. The total number concentrations for RF08CS1444 and RF08CS1553 are 11.18 and 8.12, respectively.

SD streaker results. The NASA inlet concentrations are only slight smaller than those of the TAS. Total number concentrations for RF08NS144 and RF08NS1553 are 14.55 and 11.60, respectively.

Comparison of TAS, LTI, CAI, and SD inlets. In order to compare the results from the four inlets, the data are split into four size ranges: 0.3 to 0.79 μm , 0.8 to 1.99 μm , 2.0 to 3.99 μm , and 4.0 to 8.0 μm . Above 8 μm the results are strongly influenced by small numbers of very large particles (up to about 20 μm). Table 3.4.2 show the comparative data for RF08-1553. The TAS and the LTI agree well in the first two size ranges, but the LTI shows enhancement in particles larger than 2 μm , with an average enhancement of almost 2 in the 4 to 8 μm range. The CAI has lower concentrations at all sizes, but is worst at sizes above 2 μm . The SD streaker samples have results similar to the TAS below 2 μm and somewhat lower concentrations above 2 μm . The SD inlet appears to do well with dry mineral aerosols and its performance is consistently better than that of the CAI. For RF08-1444 (Table 3.4.3) the LTI does not show significant enhancement in the first three size ranges, and shows only minor enhancement for the 4 to 8 μm range. Again the CAI did not perform well. RF08-1444 was flown at several altitudes (13,500', 12,500', etc. down to 7,500') but on average higher than RF08-1553 at 7000'. Note that both are dry FT legs. Either the ambient pressure or the operating conditions of the LTI may have affected the degree of enhancement in the larger size ranges. Size distributions for RF08-1553 and RF08-1444 are shown in Figures 3.4.2 and 3.4.3, respectively.

Table 3.4.2. Number and volume concentrations for TAS, LTI, SD, and CAI samples of RF08-1553. Number concentrations in particles/cm³; volume concentrations in $\mu\text{m}^3/\text{cm}^3$. A total of 55,270 TAS; 7,575 LTI; 28,781 SD; and 16,383 CAI particles were analyzed.

RF08T1553		TAS	LTI	SD	CAI	LTI/TAS
D _{AV} = 0.3 - 0.79	Num	5.26	5.77	4.87	3.62	1.10
	Vol	0.63	0.72	0.58	0.43	1.15
D _{AV} = 0.8 – 1.99	Num	4.84	5.57	4.39	2.97	1.15
	Vol	6.64	7.62	6.01	3.95	1.15
D _{AV} = 2.0 – 3.99	Num	1.37	2.06	1.29	0.80	1.50
	Vol	13.64	20.11	12.09	7.44	1.47
D _{AV} = 4.0 – 8.0	Num	0.27	0.56	0.28	0.15	2.07
	Vol	12.93	22.77	11.55	5.80	1.76
Total	Num	12.63	14.82	11.60	8.12	1.17
	Vol	39.97	64.91	34.35	20.62	1.62

Table 3.4.3. Number and volume concentrations for TAS, LTI, SD, and CAI samples of RF08-1444. Number concentrations in particles/cm³; volume concentrations in μm³/cm³. A total of 15,487 TAS; 13,437 LTI; 31,057 SD; and 16,383 CAI particles were analyzed.

RF08T1444		TAS	LTI	SD	CAI	LTI/TAS
D _{AV} = 0.3 - 0.79	Num	5.79	5.88	6.22	4.97	1.02
	Vol	0.69	0.71	0.74	0.58	1.03
D _{AV} = 0.8 – 1.99	Num	6.15	5.89	5.42	3.99	0.96
	Vol	8.86	8.48	7.26	5.06	0.96
D _{AV} = 2.0 – 3.99	Num	2.10	2.12	1.55	1.09	1.01
	Vol	21.65	21.34	14.58	9.98	0.99
D _{AV} = 4.0 – 8.0	Num	0.47	0.56	0.33	0.24	1.19
	Vol	20.25	24.51	13.40	9.05	1.21
Total	Num	15.47	15.46	14.55	11.18	1.00
	Vol	57.17	65.30	40.79	28.28	1.14

3.5 APS data

The identical APSs behind the three inlets offer one of the best opportunities to directly compare the relative numbers of particles passing through each inlet as a function of particle size as well as the variation of LTI performance with changing conditions. At least once on every flight all three APSs were run for 10 minutes with air from a common source (a CAI pickoff tube) as a reference so that their relative difference on the individual inlets could be assessed. Due to the low concentrations of large particles from the CAI, however, these comparisons are frequently noisy and uncertain above 7 μm. The dotted trace in some figures represents an attempt to correct the distribution from one APS that deviated most widely from the other two.

Figures 3.5.1 through 3.5.5 summarize the comparisons on each of our flight legs. Each panel represents the mean of several 5 minute average APS distributions behind each inlet. Note that the x-axis is aerodynamic diameter, with no correction for density or shape. Using the higher densities of seasalt (1-2 g/cm³) or minerals (>2 g/cm³) would move the peaks to smaller sizes by a factor of 1/ density. Particles of irregular shape would have greater drag (non-Stokesian behavior) and thus appear to the APS to be smaller than they are. Thus, their actual size would be greater than that in these Figures.

Data was stored as 5 minute averages, which makes it possible to assess the variability of ambient distributions during flight legs. During most of the MBL legs the distribution was invariant, but during some FT legs the distribution varied significantly. Examples of both can be seen in Figure 3.5.6, which shows two FT legs in dust. The right panel demonstrates that the one mode could vary widely while the other remained essentially constant.

The most obvious feature of the distributions in 3.5.1 – 3.5.5 is that the LTI virtually always had higher concentrations of particles than the other inlets. The two general exceptions are below 0.8 μm, where the APS counting efficiency is not robust, and at the largest sizes, where the number of particles was often too small to provide good statistics. It is clear that the LTI is transmitting a larger number of particles from the atmosphere to the sensors than the other inlets do, especially between 2 and 10 μm. This difference increases with increasing particle size. The extent to

which higher concentrations are due to enhancement in the LTI vs particle losses in the other inlets is discussed below.

The distribution downstream of the SD follows that of the LTI more effectively than the CAI does (usually up to about 3 μm), when the LTI concentrations become considerably higher. In cases where dry dust was present, however (panels 1-3 of Figure 3.5.5 for example), the SD and LTI distributions can be quite similar. This may be due to the tendency of dry mineral particles to bounce off surfaces and be re-entrained into the SD flow, while sea salt particles are more likely to impact and adhere to the diffuser walls. In virtually every case the CAI efficiency is the lowest of the three.

A second feature of the distributions is that the LTI usually shows two distinct modes in the volume distribution. The peak diameter of the smaller mode is around 3 μm , while that of the larger mode is in the vicinity of 7 μm . We initially questioned whether the larger mode existed in the ambient air or if it was simply an artifact caused by enhancement in the LTI and subsequent losses of the largest particles in tubing. However, we noted on several flights that the modes varied independently of one another (e.g., Figure 3.5.6), which argues that the modes are both real (even if there is some degree of enhancement). During the first leg of RF08 we observed periods of each mode by itself and other periods containing mixtures of the two. At times the 2nd mode was apparent in the samples from the CAI and SD inlets as well, though at much reduced concentrations. The sharp decrease in volume concentration at diameters greater than about 7 μm is due to two causes. First, the ambient size distribution is decreasing in concentration with increasing size as shown by the SEM analysis. Second, there is an increasing deposition rate in the inlet tubing downstream of the LTI due to inertial impaction.

To examine the variation of these two modes we fitted lognormal curves to each (Figures 3.5.8 to 3.5.19; note that these do not represent ambient modes but modes after inlet processing). Several examples showed the same features as 3.5.16, in which the larger mode is much broader behind SD than the LTI. The high-end cutoff of the LTI appears to be sharper than that of SD. That may be due to the tendency of the small-radius bend immediately behind the porous diffuser to remove the largest particles, which might successfully pass the more gentle curve behind the SD diffuser. [The need to extend a hot-film probe out the same aperture-plate that admitted the sample air necessitated this sharp bend. The ACE-Asia version of the LTI will use gently-curving concentric tubes for sample and suction flows, to avoid the sharp bend that was necessary in PELTI.]

In MBL legs the ratio of the small SD mode volume to the LTI mode volume is generally equal to that of the chemically analyzed sea salt components Mg^{++} and Na^+ , to within experimental error. For RF04 Leg 3 (Fig. 3.5.12), for instance, the SD/LTI ratios are 0.54 for Mg^{++} , 0.46 for Na^+ and 0.54 for the small mode volumes. This suggests that the small mode corresponds to the sea spray mode observed in other programs. However, the facts that 1) dry (relatively Na-free) dusty FT air also shows a mode with a peak in the vicinity of 3-4 μm and 2) this dust clearly mixes into the MBL suggest that there may also be a substantial mineral aerosol contribution to the smaller mode in the MBL as well.

The ratios of APS volume (or number) concentrations of other inlets to that of the LTI are plotted in Figs 3.5.20 to 3.5.24. Again it is clear that the LTI passes more particles in the 2 – 10 μm range than the other inlets. Even though the details of the ambient distributions differ from leg to leg, the higher concentrations behind the LTI are robust. Comparing FT legs (e.g., RF07-17:44) with MBL legs (RF07 15:36) shows that the SD/LTI ratio is closer to unity in the FT than in the MBL, presumably due to the rebound of mineral particles through the SD. These same legs demonstrate that the CAI/LTI ratio was usually somewhat better in the FT as well.

The APS observations also permit an assessment of the impact of laminar vs turbulent flow in the LTI. In RF05 there is a pair of turbulent (16:54) and laminar (16:21) legs in the MBL. The ratios in Figure 3.5.22 show that the SD and the turbulent LTI are very similar, while the SD gets many fewer particles than the laminar LTI. The larger mode in the laminar leg (Fig. 3.5.14) almost disappears in the turbulent leg (3.5.15), while the smaller mode is nearly unchanged.

We decreased the flow rate in the LTI sample tube to see if that might increase the enhancement of large particles or decrease the loss of the biggest particles in the bend behind the porous diffuser. Figure 3.5.3 (15:58) shows that the larger mode was indeed made larger when the sample flow was only 35 lpm, relative to the usual 120 lpm flow (16:21). The smaller mode height did not change between these conditions. This possible enhancement was not evident in a similar RF03 pair (35 lpm at 17:18 and 95 lpm at 17:57), which may be due to the marginal statistics at these sizes. Together these cases cannot prove there is a significant effect.

The differences between slightly subisokinetic, isokinetic, and superisokinetic sampling rates were also ambiguous. In RF05 (Fig. 3.5.3) the superisokinetic leg (17:47, 108% isokinetic) slightly de-emphasised the large mode relative to the small mode, as would be expected when pulling streamlines into the inlet tip. No difference is evident, however, between the strongly subisokinetic leg (17:30, 60% of isokinetic) and the isokinetic one (16:21, 97% of isokinetic). The same can be said of the RF03 isokinetic (17:57, 95%), subisokinetic (19:47, 78%), and superisokinetic (20:39, 111%) legs. Though possibly masked by natural variability, these small effects tend to confirm that ten percent deviations from isokinetic flow rates do not noticeably change size distributions.

3.6 FSSP-300 measurements – Darrel Baumgardner

Disclaimer: While the FSSP-300 data represents a potentially-informative comparison of two similar instruments inside and outside the aircraft, the inside configuration (the first time we are aware of anyone using an FSSP-300 in this manner) has never been calibrated for counting efficiency in the laboratory. The conversion of counts to concentrations involves critical assumptions about the nature of the flow in the sensing volume, which have not been experimentally verified. It suggests an altitude-dependent enhancement or loss (in contrast to the modeling and the TAS comparisons), but we have no way to assess the validity of the FSSP data.

The principal focus of the FSSP-300 measurements was to determine how well the LTI passes super-micron particles. Hence, the analysis deals only with comparisons between the probes of concentration and volume in the nominal size range of 1 – 20 μm in the two probes. The FSSP-

300 has 31 size channels. The lower size threshold of channel 13 is $0.95\ \mu\text{m}$, its upper size threshold is $1.140\ \mu\text{m}$. This threshold varies quite a bit, depending upon the actual refractive index, but for the purposes of these measurements, the concentrations and volumes will be determined between channels 13 and 31 of each probe.

In order to determine any differences between probes, unrelated to the effects of the LTI, the two FSSP-300s were flown outside the aircraft on the ferry flights (RF09 and FF02) returning from the field site. One probe, the NASA probe, was mounted on the left pod and the NCAR probe was mounted on the left wing-tip. Figure 3.6.1 shows average size distributions from both of the probes over the size range greater than $1.0\ \mu\text{m}$. Both MBL and FT data are shown. This demonstrates that in the free stream the two instruments are in good agreement for number concentration. The factor-of-two differences in certain channels may be due to counting statistics, which we have not yet been able to assess quantitatively.

Figure 3.6.2 illustrates a number of features of the cabin to wing FSSP-300 comparisons, using averages over one MBL and one FT leg. If we first look at the concentrations in the boundary layer (left side of the figure) we see that the cabin FSSP is usually but not always higher than the wing FSSP, making the cabin/wing ratio generally greater than 1, in some cases by a factor of 10. In the FT (right panels) by contrast, the wing FSSP concentrations are greater than the cabin below about $8\ \mu\text{m}$, above which they switch. The cabin/wing ratios vary in different ways on these two legs, but each leg has sizes with ratios both greater and less than 1. The reasons for this are not evident at this time, but we suspect it has to do with the nature of the flow in the cabin FSSP sensing volume.

The flow rate through the LTI was varied from leg to leg to assess the impact of the internal flow rate. The FSSP-300 measurements were stratified with respect to these different flows in Figure 3.6.3 for Flights 5-8. In this figure, the plotted number equals $1/10$ of the flow rate in lpm. It is evident that the ratio of the external to internal FSSP volumes depends on both altitude (the 40 lpm points are illustrative) and on flow rate in the internal FSSP. We are unable to explain this behavior.

Since we do not understand the relationship between the flow rate and apparent concentration in the cabin FSSP, we cannot defend the observed ratios. Thus, we cannot use the FSSP data in drawing conclusions about the LTI performance.

3.7 Lab measurements of losses in tubing

Obviously, the fidelity (to ambient) of the aerosol distributions measured behind each inlet is a function of both the inlet efficiency and the passing efficiency of the tubing that conveyed particles from that inlet to its samplers. We are using a vibrating orifice aerosol generator (VOAG) to make monodisperse uranine dye particles for directly measuring the size-dependent efficiency of each section of tubing (Blomquist et al., 2000). After passing each size of particles through a section of tubing and collecting the particles that are passed through it, a spectrofluorometer is being used to measure the amount of uranine in the extract of each section. In this way, we are deriving loss-vs-size curves that will be used to isolate the separate impacts of the tubing and the inlet.

Since the shipment of interior tubing from PELTI did not arrive in Hawaii until 24 August, it was not possible for us to complete the laboratory tests of the passing efficiency of this tubing prior to the submission of this report.

3.8 Modeling of enhancements using Fluent

The LTI reduces turbulence in the diffuser cone and greatly reduces the unquantifiable impact of turbulent deposition to the walls of the diffuser cone. However, the aerosol samples acquired with the LTI are not necessarily representative of the ambient aerosol. Two effects must be considered. The slowing of the air in the inlet will result in heating of the sample due to adiabatic compression. This heating occurs in all inlets that slow the flow, and the amount of heating is identical in inlets in which the flow is slowed by the same amount. The second effect is an inertial enhancement of particles with large aerodynamic diameter. Inertial enhancement results from the rapid bending of streamlines in the diffuser as the area expands and as most of the air is sucked through the porous diffuser wall. Particles unable to follow the bending streamlines are concentrated in the sample flow that exits the rear of the diffuser. The inability to follow the flow increases with aerodynamic diameter.

Numerical calculations have been used to determine the enhancement. This modeling was done by David Gesler and Chuck Wilson of the University of Denver. The flow is first calculated using equations that include the effects of compressibility and the porous material. Then particle trajectories are calculated by integrating the laws of motion. The particle drag coefficient includes the impact of particle Reynolds numbers that are outside of the Stokes regime. Calculations of this type have been used to accurately describe several situations involving laminar flows and particle motions. The list includes: 1) the performance of inertial impactors (Marple and Liu, 1974), 2) the use of velocimetric measurements to determine aerodynamic diameter (Wilson and Liu, 1978), 3) the impact of aerosol density on the performance of the TSI Aerodynamic Particle Sizer (Anath and Wilson, 1988), 3) the impact of anisokinetic sampling with blunt tubes (Rader and Marple, 1988), and 4) the loss of particles in bends (Pui et al., 1987). By contrast, in most solutions of turbulent flow, the mean velocities are calculated and the fluctuations that actually account for the particle deposition are parameterized. Unlike numerical approximations of aerosol deposition in turbulent flow, the laminar calculations described here do not involve parameters that can vary from case to case and thus change the results.

The laminar flow through and particle trajectories in the LTI have been calculated using the CFD code Fluent r5.2.3. The axisymmetric geometry and boundary conditions are shown in Figure 3.8.1 (dimensions in inches). Grids were generated using the Fluent preprocessor, Gambit. The grid close to the internal walls is finer than that of the core flow to allow for viscous wall effects to penetrate the core flow. An example is shown in Figure 3.8.2. Finer grids have been evaluated; the calculated results do not change with grid size.

It should be noted Fluent does not recognize porous media as a wall but rather models it as a sink in the momentum equations. The porous media sink is determined using Darcy's Law for viscous losses given by:

$$\frac{P}{x} = \frac{\mu}{\rho} V_i + C_2 \frac{1}{2} \rho V_i^2$$

where μ is the gas dynamic viscosity, ρ the gas density, V_i the average normal velocity of the flow passing through the porous media, $\frac{\mu}{\rho}$ the viscous permeability coefficient and C_2 the inertial loss coefficient of the porous media. The values of $\frac{\mu}{\rho}$ and C_2 were determined empirically for this diffuser were $7.752e-12 \text{ m}^2$ and $1.78e6 \text{ m}^{-1}$ respectively. This choice of parameters results in the same splits between sample and suction flow as that are seen in the operation of the inlet.

Two data points were evaluated from two different flights. The corresponding boundary conditions used in the calculations are given in Table 3.8.1.

	186rf03 74350<UTS<74950	186rf07 65501<UTS<66500
Ambient Total Pressure (Pa)	109446	80923
Mass Flow @ Inlet (kg/s)	0.0167	0.0116
T @ Inlet (K)	294.8	284.4
Static Pressure @ Core Outlet (Pa)	107118	80832
T @ Core Outlet (K)	306.6	293.7
Static Pressure @ Suction Outlet (Pa)	90246	67923
T @ Suction Outlet (K)	306.5	295.7
Suction/Total Mass Flow Split	0.855	0.772
Isokinetic Ratio	1.106	0.864

Table 3.8.1. Flight Data/Boundary Conditions for CFD Calculations

The laminar and compressible internal flows were first calculated. Particle injections were then generated. The injections represent a spatially uniform concentration of 1000 particles with density 1.6 g/cc and varying diameters that enter the calculation domain at the mass flow inlet with the same velocity and direction as the entrance flow. Diffuser passing efficiencies for particles in the diameter range from 0.1 to 11 micrometers diffuser were calculated. The diffuser passing efficiency equals the percentage of particles entering diffuser that are present in the sample flow. A sample is representative of the ambient aerosol when the diffuser passing efficiency equals the percentage of inlet flow which is present in the sample flow. The calculations include particle drag coefficients which accurately represent drag on spheres both inside and outside of the Stokes regime. The use of ultra-Stokesian drag is necessary because the

particle Reynolds numbers exceed 0.1. The entrance and exit mixing ratios were calculated from the passing efficiency and the entrance and exit mass flows. The corresponding enhancement factor and diffuser passing efficiencies are plotted against aerodynamic diameter in Figures 3.8.3 and 3.8.4. Note that non-unity efficiencies for submicron particles are a statistical artifact, resulting from the fact that only 100 particles of each size were modeled to conserve computing resources.

In both cases, particles larger than 1 micrometer experience mixing ratio enhancements at the diffuser exit. Particles smaller than 1 micrometer experience exit mixing ratios that are representative of the ambient. Figure 3.8.4 shows that the enhancement calculated for flight conditions at low altitude agreed well with those calculated for flight conditions at higher altitude. Thus, the enhancement factor is not a strong function of aircraft altitude.

Figure 3.8.3 includes curves which combine the enhancement with particle losses expected in the bend that immediately follows the diffuser. Both laminar flow calculations and empirical correlations from turbulent flow measurements (Pui et al., 1987) were used to estimate the bend losses. The Reynolds number in the bend was approximately 8000 but the entering flow was laminar. It is not clear which formulation should be more accurate; however, the results did not differ by much. These estimates did not account for the fact that the radial distribution of particles exiting the diffuser is not uniform, so the losses may be exaggerated. It is also likely that in dry dust, bend losses will be reduced by particle bounce off the walls. These curves also do not include estimates of losses in the tubing between the inlet to the aircraft cabin and the filter sampler. These losses are not expected to be large but may approach several percent for supermicron particles.

The effect of the blunt leading edge external and probe geometry on aspiration coefficient have not yet been evaluated. LTI isokinetic sampling is defined as occurring when the velocity at the blunt leading lip equals the free stream velocity. In this condition, the throat velocity is faster than the free stream velocity by about 16%. During the filter samples, the average ratio of LTI flow to the isokinetic flow was 0.94. Thus the throat flow averaged 1.1 times the free stream flow. Theoretical work suggests that the blunt leading edge may reduce the sensitivity of the of the sampling efficiency to the minor velocity mismatches seen here (Rader and Marple, 1998).

In order to determine the ambient mass mixing ratio for the analyzed ions on the filters, it is necessary to combine the effects of anisokinetic sampling, inertial enhancements in the diffuser, losses in the bend and losses in transport from the bend exit to the filter. These effects depend on aerodynamic diameter of the particles sampled. The APS measurements and curve fits suggest that the geometric mass mean aerodynamic diameter fell between 4 and 5 microns for the measurements displayed above. The maximum anisokinetic and diffuser enhancements for 5 micron particles combine to about 17%. Conservative estimates of bend loss and transport loss combine to losses near 10%. Thus, the mass mixing ratios determined from the filters behind the LTI could exceed the ambient values by about 10%.

A more detailed treatment of the radiative impact of various losses and enhancements can be found in section 4.2. These corrections are applied to APS data in Section 3.9 to see estimate the

ambient scattering. Otherwise, no data in this report has been corrected for enhancements and losses unless the text specifically states that this correction has been made.

3.9 Nephelometers

One of the purposes of PELTI was to compare the suitability of the inlets for capturing a sufficiently representative aerosol to permit accurate calculations of aerosol optical properties. To that end, Figure 3.9.1 shows the CAI and SD nephelometers (corrected for the common-inlet calibrations) plotted against the LTI nephelometer. As would be expected from the APS size distributions, the CAI gathered enough aerosol to produce only 72% of the scattering signal of the LTI. The solid diffuser produced scattering values roughly 87% of the LTI in the average, which is consistent with the chemical and APS data. Note that these data have not been stratified for wet or dry conditions.

A full treatment of this topic is not possible in the time available, but there are two likely reasons for the lack of more enhanced scattering in the LTI. The first is that mass scattering efficiency peaks at about 1 micron. The SD and LTI size distributions generally agree well up to 2 or 3 microns, so the LTI enhancement at larger sizes involves too few particles to affect scattering by more than about 10%. In addition, large particles scatter primarily in the forward direction, where the Radiance Research nephelometers we used are insensitive. This so-called truncation error can be corrected with sufficient knowledge of the size distribution and nephelometer geometry, but we did not have the time to do so for this report.

The impact of the LTI and SD on scattering can be seen in Figure 3.9.2, in which the LTI APS data is corrected for enhancement using the Fluent results, and both the LTI and SD are corrected for losses in the long transport tubing. The upper panels are the raw and corrected volumes from both inlets, for dust and seasalt legs. The middle panels show the predicted scattering with size from each inlet, while the bottom panels show plot the cumulative scattering from both. The difference between the two is on the order of 10% in the dust case and 20% in the sea salt case. The impact of the low mass scattering efficiency of the largest particles is evident as the flattening out of both cumulative scattering curves in the 7 – 10 μm region. Thus, a failure to sample these largest particles quantitatively will not degrade light scattering measurements.

The relatively poor performance of the CAI has some consequences for evaluating data from previous experiments. For calculating optical properties, PELTI was nearly a worst-case scenario, with scattering due primarily to large, difficult-to-measure particles. That was not the case for INDOEX, where scattering due to submicron pollution particles generally dwarfed the dust and seasalt signals to the extent that a large error in sampling large particles would have little effect.

That was not the case for ACE-1, where the remarkably low pollution levels around Tasmania meant that seasalt was the primary source of scattering in the marine boundary layer.

4. Discussion and Critique of Methods

4.1 Tasks remaining

Several important tasks remain unfinished. Perhaps the most obvious is the laboratory measurement of particle losses in the tubing used to move particles from inlets to instruments. That will allow us to be more certain of the enhancements caused by the LTI. Another is the SEM analysis of more samples, to increase the number of TAS/LTI size distribution comparisons. The two samples run so far show quite different enhancements (20% vs 100% at 8 μm); with just two samples it is not possible to determine which of these is more common. However, this kind of analysis is costly and time-consuming, so we may not be able to have all the samples analyzed.

An important task that we do not have the resources to do is to calibrate the FSSP-300s for concentration, rather than just sizing. This is critical as we are to continue using these devices in a quantitative manner. We also need research on the use of the FSSP in cabin-mounted configurations, since this should permit useful comparisons with ambient concentrations. The nature of the flow in these configurations needs considerable study.

Since the reader must make judgements about which types of observations to put more or less confidence in, we critique below each of the measurements and models used in the assessment of the LTI. Each critique is signed, so that readers can judge the comments against the experience of the author.

4.2 Critique of the APS data – Dave Covert

The starting point for the assessment of the APS measurements is a comparison of the data from the three instruments when they sampled in common from the CAI inlet. This inlet was chosen as the reference because we had most experience with it and it could provide adequate flow for all three modules. In retrospect we would have obtained better counting statistics if we had used the LTI as the common reference inlet for the APS samples. Small deviations noted during the calibrations were used to correct the flight data.

The three APS units were tested at the RAF hangar (in the aircraft on the ground) prior to the PELTI campaign and again afterwards for flow rates, relative counting efficiencies with latex sphere particles, and particle sizing. The pressure dependence of the flow control and sizing were tested as well. Flows and sizing were within a few percent of the nominal values and were independent of pressure from 950 to 600mb.

Ideally the three APS would have indicated the same particle concentration over the size range 1 to 10 μm when operated on the CAI. From Figures 3.5.20 through 3.5.24 it is clear that when operated on the common CAI inlet during PELTI flights, the concentrations measured by the three units varied by $\pm 20\%$ over the range 1 to 7 μm . Differences above 7 μm were much larger and likely due to poor count statistics. The observed differences in the range 1 to 7 μm are larger than can be attributed to uncertainties in the flows or sizing or counting efficiencies of the instruments based on ground testing of the APSs. Thus, the test of whether the three APS unit

agreed within their uncertainties was negative. Either flight conditions caused the errors in the APS to increase or the loss of particles in the flow distribution plenums and plumbing from the CAI to the three APSs was not identical and varied with flow conditions. Lab tests of the distribution plenums may shed more light on this potential factor. Flow rates and alignment in the APS may change with varying inlet and outlet pressure and aircraft vibration which would affect counting efficiency and sizing. In-flight calibration of flow, counting efficiency or sizing was not attempted. We relied on the APS's internal sensors and feedback circuitry to maintain constant flow.

However, the differences in concentration measured by the three APSs when operated on the individual CAI, LTI and SD inlets during PELTI was much greater than the 20% difference between units when operated on the common inlet. Thus, we can be assured that the conclusions about the relative passing efficiency of the inlets (and the enhancement factor for the LTI) are valid and quantitative within the uncertainty determined by the common inlet tests.

The calibration and counting efficiency of the APS have not been studied rigorously in the laboratory or under real field experiment conditions to determine accuracy, time stability and pressure dependence of its operation.

4.3 Critique of anion and cation data – Barry Huebert

On one hand, it seems that analyses from TAS should be the most fundamental data upon which to base an analysis of the LTI efficiency: Everything that enters the tip gets analyzed. If a particle sticks on the cone wall or on a filter, it gets extracted and analyzed. The total can be defended for lack of bias from sampling losses.

However, this measurement is the opposite of a continuous instrument. One must clean the cones and filters carefully, transport them, open them in a dirty airplane, and then extract the deposited analyte, all with minimal contamination. It involves a lot of manipulations under field conditions. The result is that TAS won't ever give as fine a precision as a single filter. It is possible to define its accuracy, though, in a way that is impossible for many other methods. Some examples of blanks are tabulated below.

Nanograms of Analyte on Field Blanks	TAS Cone Blanks Flights 4-8 Ca⁺⁺	Teflon Filter Blanks Flight 8 Ca⁺⁺	Teflon Filter Blanks Flight 4 Na⁺
	1484	250	1080
	1499	250	591
	1050	287	1860
	1898	275	4387
Average	1483	348	1210
Std Deviation	± 346	± 40	± 1502

The Teflon filter blank variability is just ± 40 ng Ca⁺⁺, while the TAS cone-wash blank variability is ± 346 ng Ca⁺⁺, an order of magnitude larger. Thus, there will be more scatter in the TAS data than for the other samplers even though its bias is minimal. For some lots of filters,

however, there is a large and erratic blank variability such as that found during PELTI for Na^+ : 82% of the blank average. It is this blank variability that in practice limits the accuracy of the anion and cation data. Generally the IC detection limit is not an issue for most species, nor is its calibration: every 5th sample in the IC is a standard and the extracts being compared have similar concentrations of analyte. However, collecting enough sample in a short time (30 to 60 minutes is a long aircraft sample) to exceed the blank variability can be difficult. When we collected 25,700 ng of Na^+ on one leg of RF04, the large Na^+ blank variability was not a serious problem, but for many other legs it severely limited our precision. The error-boxes on the chemical figures include 2x the blank variability, the detection limit for that species, plus 5% for flow uncertainty. (These filters can and will be pre-washed to reduce this variability.)

The other major factor limiting the accuracy of comparisons between filter samplers is the measurement of the volumes of air sampled. Thermal mass flowmeters can have an accuracy of several percent, but they must be calibrated often. It is particularly important that they be intercalibrated by running them in series under the conditions of flight, so that any pressure or temperature sensitivities can be calibrated out. In this way we feel confident that the 5% uncertainty we assign to the flow through each filter is very conservative. Two to three percent is probably the relative uncertainty after those intercalibrations have been applied to the flow data.

It is difficult to combine all the individual sample uncertainties and the variability between samples to achieve a single percentage uncertainty. However, we believe the accuracy of the average ratios of the LTI filters to TAS is less than 20% for most species and may approach 10% for Cl^- and Mg^{++} .

[We are happy to share the IC/filter spreadsheets with anyone. huebert@soest.hawaii.edu]

4.4 Sources of error in SEM analysis – Jim Anderson

Sizing: Why do the SEM- and APS-derived size distributions differ? To start with, there are several possible ways to define a size parameter from the SEM two-dimensional measurement of three-dimensional particles: one can average 2-D maximum and minimum dimensions (D_{\min}); one can take the square root of the 2-D area; or if the Z dimension is similar to the dimensions in X and Y, one can assume that $Z = D_{\min}$ to extend the 2-D area measurements to volume (from which we derived our 3-D effective diameter). How well do any of these approximate reality? Confounding our 3-D approach is the fact that particles tend to lay flat on a filter: in cases where the Z dimension is substantially smaller than D_{\min} , the derived 3-D parameters will be unrealistic. The magnitude of their error can only be assessed qualitatively.

The PELTI dust samples are unusual in that many (not all) of the particles are rather flat, tabular particles of clay. This effect is seen over the entire size range and tends to shift the volumes derived using D_{\min} to larger sizes. These samples are not like typical desert dust, but more likely are from a clay-rich topsoil being blown off an area impacted by over-grazing or other poor farming practices. The atypically flat shapes also impact optical measurements of particles (such as the FSSP), since light scattering is related to surface area. If tabular particles become oriented in the air stream the laser beam may be scattered by a much larger surface than if a particle of the same volume was spherical (which the optical analyses assume). Further, the flat surface may be

much more efficient at scattering light to the detector than a sphere with a similar projected cross-sectional area. Thus both SEM and light scattering methods may oversize tabular particles. Methods based on aerodynamic drag, by contrast, will undersize these particles since their complex shapes will cause them to follow the streamlines like smaller particles do.

While this sort of problem may explain some of the differences between the APS and SEM measurements, the presence of some flat particles at all sizes should primarily shift the number size distributions for the SEM not just broaden them. However, the volume size distributions from the SEM should be broadened as the error is greatly amplified in calculating volumes. Non-ideal sizing by the APS at the smallest and largest sizes must also play a role in generating the observed differences.

Concentration: Three main considerations determine the error in concentration: (1) how uniform is the loading on the filter and - if not uniform - was enough of the sample area analyzed to be representative; (2) how well is the sampled air volume known; and (3) for a given size bin were enough particles analyzed to represent the entire population. The streaker filters have uniform loading, but the TAS filters do not, as discussed above. The error in the flow measurements for the streakers may be on the order of 10% due to the calibration changing over time. On future experiments where we expect to encounter potentially corrosive aerosols, the calibrations may need to be done more frequently.

Validity of TAS-LTI comparison using SEM: The problems with shapes does not affect the comparison of SEM data between inlets except to the extent that it might change the apparent size at which loss or enhancement occurred. The errors in air flow would move the distributions up or down but not change their sizes. The fact that the SEM results from TAS and the LTI agree very well below 2 μm gives us confidence that this flow error is small. It appears, however, that the CAI under-performs the LTI at all size ranges since its small-particle deficit is greater than our estimated flow uncertainty.

The shape problem does affect our ability to compare the SEM results with the APS and FSSP results. To our knowledge, this is the first time that quantitative single-particle data has been compared with aerodynamic and optical instruments such as the APS and FSSP in dust. Each method uses different principles for defining “size” that make perfect agreement among the methods impossible. Even simple comparisons of particle number concentration are complicated because the size bins of each instrument do not correspond to exactly the same sizes in the SEM data. This disagreement between methods is to be expected. PELTI has been a very informative exercise that is helping us to refine our understanding of particle size for use in future projects.

4.5 FSSP data concerns – Antony Clarke

The PELTI strategy for testing the LTI included comparing a wing mounted FSSP [Forward Scattering Spectrometer Probe] and a cabin FSSP downstream of the LTI, with the intention that both external and internal measurements could be made and compared using similar instruments. The plan was to directly compare ambient and aspirated (LTI) size distributions so that “absolute” LTI transmission performance could be assessed. These FSSP’s were both configured so that they could be mounted on the wing together and compared, which was done.

They could also be interchanged, which was also done. Side by side performance while on the wing was within expected uncertainties (estimated by Darrel Baumgardner to average about 22%) and relative performance when swapped inside vs. outside was similar, suggesting both FSSP's were performing within expected performance limits at each location and that no instrument problems were evident per se. Larger bin to bin concentration differences evident for size bins above about 5 μ m (Figure 3.6.1) may be driven by sample statistics rather than instrument or calibration uncertainties.

However, in spite of apparent instrument functionality, the data from the internal FSSP behind the LTI was generally far different in its measured concentrations and resulting size-distributions than would be expected. Moreover, at times both individual size distributions and their integral number and volume distributions (particularly for supermicrometer aerosol) for the internal FSSP far exceeded the external probe while at other times they were far less than the external probe. Most significantly, large excursions in apparent internal FSSP performance behind the LTI were not reflected in any of the other instruments sampling behind the LTI (APS, nephelometer and SEM data) or in their comparison to the external TAS data.

Because flows inside the FSSP were varied from 30 to 80lpm for different flights and at different altitudes, efforts were made to stratify internal/external FSSP relative performance. Plots of relative performance (Figure 3.6.4) indicated the most inconsistent performance between internal and external FSSP occurred for the higher flow rates, pointing to flow in the internal FSSP as a possible confounding factor. If only the lower flow (40 lpm) data were used, then the variations in relative performance with altitude at least intimate a regular trend. This trend implies a tendency for the internal FSSP to have two to three times higher concentrations than the external FSSP at low altitude (below 1 km) but to approach similar concentrations as the wing probe at higher altitudes (3 km). However, even with this flow stratification, similar or related behavior is not evident in the other instruments or in their relationship to TAS, the other external sampler. Comparisons of internal/external FSSP size distributions still indicate inexplicable shifts behavior and even crossover (undercounting in smaller sizes and overcounting in larger sizes). Also, factors of 3 or so differences evident between internal/external FSSP concentrations near or below 1 μ m diameter are disturbing, where both FLUENT modeling results and previously measured inlet effects argue the differences should be small. Further analysis (D. Baumgardner) indicated that these differences could not be accounted for by FSSP electronic "roll off" related to differences in ambient and internal FSSP sample flows.

As suggested by the discussion above, this unexpected behavior is probably not related to the internal FSSP instrument itself but instead to the way its sample flow had to be modified for use inside the aircraft. The normal large diameter "throat" of the instrument had to be "plugged" at the inlet and outlet of the scattering region. Flow was accelerated and passed through small orifices in the plugs that opened into the laser cavity. This is similar to the approach used to prepare the instrument for calibration in the laboratory. However, such calibrations are performed at only one pressure and are designed to establish the size discrimination of the instrument. To our knowledge there have never been evaluations of the size dependent counting efficiency (concentration) when the FSSP is operated in this configuration. Details of the "jet flow" (eg. possibly greater variation and uncertainty in axial and radial velocities, cross sectional area, turbulence, particle alignment etc.) of the air from the small inlet to the detection region

and possible changes with altitude (pressure) may impact concentration measurements more than size. Both this untested configuration for the assessment of concentrations and the fact that the FSSP data includes many inconsistencies that are not presently understood (and are not evident in other instruments) makes the FSSP data suspect. It should be discounted in the final PELTI analysis.

4.6 Net LTI Passing Efficiency – J. C. Wilson

In order to relate measurements made down stream of the LTI to ambient aerosol properties, it is necessary to know the passing efficiency of the LTI and associated plumbing. The net passing efficiency is defined as the aerosol mass mixing ratio in the sample delivered by the inlet divided by the aerosol mass mixing ratio in the free stream. The net passing efficiency is probably a function of aerodynamic diameter and density with aerodynamic diameter accounting for most of the variability. The passing efficiency is determined by fundamental considerations of flow and particle motion. The PELTI measurements are very useful for validating the net passing efficiency determinations. The net passing efficiency for PELTI will include the effects of inertial enhancement in the diffuser, the effects of anisokinetic sampling at the diffuser entrance, and the effects of losses in the plumbing between the diffuser and the filter or instruments. The APS measurements from PELTI that were analyzed for this report showed aerodynamic mass median diameters between 4 and 5 microns. Assuming that these distributions represent the aerosol collected on the PELTI filter samples, a representative, net LTI passing efficiency for particles with an aerodynamic diameter of 5 microns was estimated for application to the filter collections. This LTI passing efficiency was found to be 1 ± 0.2 . This estimate permitted the direct comparison of the filters collected behind the LTI with the TAS. The accuracy of the passing efficiency estimate is limited by the uncertainties in the estimates of transport losses, the uncertainties in the estimates of the inertial enhancements in the diffuser and uncertainties in the impact of anisokinetic sampling. Each of those factors is discussed here.

The inertial enhancements in the diffuser are calculated numerically using Fluent (Section 3.8). Since the inlet maintains laminar flow and the free stream turbulence is usually quite small, the flow calculations use the equations governing laminar flow. The drag coefficients used for the calculations include the effects of ultra-Stokesian flow. Laminar flow calculations have resulted in accurate predictions of spherical particle trajectories (Marple and Liu, 1974, Wilson and Liu, 1980, Ananth and Wilson, 1988, Rader and Marple, 1988, Tsai and Pui, 1990). Insufficient grid density, overly large integration steps in the particle trajectory calculations and incorrect drag coefficients can lead to errors. These issues have been addressed in the present calculations by increasing grid density, reducing step size and by checking particle Reynolds numbers. The particle Reynolds numbers were well outside of Stokes Regime but within the range covered by the drag coefficient correlations. The grid and step sizes were reduced without change in the result. Thus, the calculations meet the tests that are usually applied in this type of analysis. The ultra-Stokesian drag implies that the enhancement will depend on particle density as well as aerodynamic diameter (Ananth and Wilson, 1988). The density effect is expected to be small, but has not yet been explored. The calculations were done for particles with a density of 1.6. Laboratory validations of the enhancement calculations are difficult and have not been done.

The numerical calculations do not yet include the coupled flow around the inlet and into the inlet. Such calculations would account for the effects of anisokinetic sampling in the geometry used in the LTI. Rader and Marple (1988) showed that a blunt inlet performs like a thin-walled inlet in superisokinetic sampling. Using the throat velocity, the ratio of sample flow to that needed for isokinetic sampling varied from 0.76 to 1.26 in PELTI, and the average ratio was 1.10. The average aspiration ratio predicted for thin walled inlets for particles having an aerodynamic diameter of 5 microns is 0.94. This estimate suggests that the effects of anisokinetic sampling are small in PELTI and that they tend to reduce the effect of the inertial enhancements in the diffuser.

Losses in transport also tend to reduce the effect of the inertial enhancements in the diffuser. Estimates based on published experimental correlations suggest that these losses are less than the enhancement in the diffuser. Figure 3.8.3 includes estimates of the losses in the 90 degree bend that follows the diffuser. Losses from both laminar and turbulent flow are plotted. The actual flow probably transitions from laminar to turbulent in the bend and the spatial distribution of particles entering the bend is probably not uniform. The predicted losses are not large for particles having 5 micron aerodynamic diameter. The deviation from the assumed conditions is not expected to increase the losses from the predicted range. Steven Howell at the University of Hawaii estimated the losses in the plumbing following the bend and preceding the filter holder. His estimates for losses of 5 micron particles are on the order of several percent but are not large compared to the inertial enhancement. Experimental studies of transport losses are planned at the University of Hawaii. Efforts are underway to avoid the 90 degree bend following the diffuser in ACE-Asia. This would reduce uncertainties in passing efficiency.

The largest effect is the inertial enhancement in the diffuser. That is also the best understood at this time. Reasonable estimates of the impact of anisokinetic sampling and losses in transport reduce the LTI passing efficiency at 5 microns to around 1.1. The value of 1 was chosen to permit direct comparison of filter measurements and is certainly within the error bars. Improvements in these estimates are planned, but the effects are sufficiently well-understood to say that significant changes are not expected.

4.7 What does “particle size” mean? – Steve Howell

One of the unusual features of the PELTI project is our redundant instrumentation. We are examining the performance of the LTI with 5 quite different measurement techniques: optical particle counters, electron microscopy, bulk chemistry, aerodynamic size, and nephelometry. As anyone who has participated in an intercomparison would predict, each set of instruments tells a different story about the LTI performance. We do not yet understand the very large enhancements shown by the FSSP. There is a rough agreement between the other methods that the LTI collects more particles than the other inlets, and that enhancements are not as large as the factor of 4 worst-case model prediction for the LTI. When trying to reconcile the different methods, we run into problems like the distributions shown in figure 4.7.1. While SEM and APS number distributions show very similar overall concentrations and median diameters, the SEM distribution is lower and broader. When calculating particle volume this difference is magnified to a disagreement of a factor of 2 or more. The 6 micron mode evident in the upper right APS plot is apparently absent in the SEM distribution.

These differences are beyond any reasonable uncertainty due to flow rates or size calibration in either the APS or the SEM. Although we have not yet developed quantitative means to demonstrate this, the difference appears to be due to the physical means each uses to measure particle diameter and volume. Each number distribution is 'correct' given the appropriate definition of diameter.

An APS measures the speed of particles accelerated through a small jet. That speed is determined by the aerodynamic force on the particle and its mass. Sizes are generally reported as aerodynamic diameter, i.e., the diameter a spherical particle of unit density would need to have the same speed at the exit of the jet. The relationship between physical diameter and aerodynamic diameter for spherical particles can be calculated; it is approximately the square root of the density. (Turbulent flow occurs around large particles in the jet, requiring an additional correction for "ultra-Stokesian drag".) This is satisfactory for liquid aerosols, but solid particles are often non-spherical, have more aerodynamic drag, accelerate faster, and thus appear smaller than spherical particles of the same mass. Figure 4.7.1 has been corrected for an estimated particle density of 2.6 g/cc but not for any effect of shape, so it is not surprising that the APS undersizes large particles. This underestimation of diameter may have a severe effect on volume calculations, which depend on the third power of diameter. Without some kind of shape correction, volume calculations from APS data must be considered questionable.

Aerodynamic diameter does have some uses, as it is a measure of the interaction of particles with the air, so is useful for calculating settling velocity. It is also the property that governs the behavior of a particle in an inlet. Hence, enhancements in the LTI and losses in tubing and the other inlets should be functions of aerodynamic diameter.

The FSSP and OPC measure the quantity of light scattered from a laser beam over a certain solid angle. Even in the simplest case, spherical particles with known index of refraction, the relationship between diameter and scattering is not monotonic; more than one particle diameter can cause the same amount of scattering. (For the wavelength of the HeNe lasers used in the FSSP and OPCs, this problem is most pronounced in the range of 1 to 2 microns.) Mie theory can be used to calculate the effects of changing refractive index, but is extremely difficult to apply for particle shapes other than spheres and long rods. Consequently, the 'diameters' produced by these optical counters is a parameterization only indirectly related to the physical dimensions of the particles. This parameterization is exactly what one wants when calculating the optical properties of the aerosol, nephelometer measurements often agree with those calculated from OPC size distributions (Clarke et al., 1995).

In contrast, the SEM analysis allows us to measure size directly from the image of a particle. While this simplicity is appealing, there are issues that remain unresolved. First of all, since the SEM work requires a vacuum, all volatile materials are lost. Many particles, particularly in the MBL, are primarily water, volatile sulfates and nitrates, and perhaps volatile organic materials. Therefore the relationship between the SEM image and the particle under ambient conditions can be difficult to determine. Because of this, we have concentrated on dust samples, where we expect the particles to be less affected by vacuum. Note that loss of volatile material tends to bias SEM estimates down from ambient sizes so cannot explain the differences in figure 4.7.1.

Another problem is that the SEM images are 2-dimensional; we do not get particle depth directly (this could be overcome using atomic force microscopy or related techniques, but those are far too time-consuming for this report). We calculate volume by assuming that particle depth is equal to the minimum width of the image. This is an admittedly crude assumption, but seems as reasonable as anything else.

Despite these difficulties with the SEM analysis, it gives a far richer description of the nature of aerosol particles than the crude parameterizations of diameter provided by the APS and OPC. It reveals that a single dimension parameter is absurd for many of the solid particles encountered during PELTI (see Figure 3.4.1 for a good example). While it is as yet unclear how to best to use the SEM particle dimensions in volume, scattering and aerodynamic diameter calculations, it is far more difficult to convert APS data to optical diameter or OPC data to aerodynamic diameter.

The contention that particle shape is primarily responsible for the differences between APS and SEM distributions requires that the undersizing by the APS is worse for big particles. That could only be true if the larger particles have more complex shapes and therefore more aerodynamic drag. This is indeed the case, as shown in Figure 4.7.2. Circularity is a shape factor calculated from the area and perimeter, normalized so a circle has a circularity of 1.0 and more complex shapes have higher values. As Figure 4.7.2 demonstrates, small particles were very nearly circular and shapes became more irregular for larger particles. Thus the APS undersizing should be exacerbated for big particles, as is the case in Figure 4.7.1. It may be possible to use circularity or some similar shape factor to approximate aerodynamic or optical diameters from the SEM data, but we have not yet developed any quantitative relationship.

It appears that the most appropriate measure of diameter depends on the calculations in which diameter needs to be used. Aerodynamic diameter is useful for describing behavior of particles in the atmosphere and within inlets while optical diameter works for calculating scattering and other optical properties. None of these methods are adequate for finding particle mass, though the SEM comes closest (for non-volatile particles), particularly when combined with EDS analysis to determine particle composition. Cascade impactors classify particles by aerodynamic size, but can be used to determine integral mass, so are probably the most direct means of determining mass fluxes due to aerosol deposition. A single parameter (such as diameter) may be inadequate for some of the uses to which particle size information is put.

When working with the PELTI data it became clear how strikingly different these size distributions can be. When we use one type of size to estimate a different type of effect, we may seriously misrepresent reality.

5. Recommendations and Conclusions

5.1 Comparison of inlets

Hypothesis A: The LTI has a demonstrably higher aerosol sampling or transmission efficiency than both the CAI (the NCAR C-130 community aerosol inlet) and traditional solid diffusers for particles in the 1-7 μm range.

Conclusion: *It is clear that the Hypothesis A cannot be disproven: the LTI consistently had larger concentrations of particles than the SD or the CAI.*

However, we note that our real goal is to achieve efficiencies near unity. The ubiquity of losses in earlier inlets lead us initially to state this hypothesis in terms of "higher" efficiency, but enhancement by the LTI may in some cases cause efficiencies substantially above 1. Since enhancements in laminar flow are calculable many measurements can be corrected for them, but the "highest" efficiency is not necessarily the most desirable one.

We base this conclusion on the following evidence:

- On virtually all legs the LTI APS distributions rose above those of the SD and the CAI. The only exceptions are very small and very large particle sizes, for which measurement errors are prominent. The advantage over the other inlets increases with particle size from 2 to about 8-9 μm .
- On virtually all legs the concentrations of anions and cations were greater on Teflon filters behind the LTI than on similar filters behind the SD and CAI and on an impactor behind the CAI.
- The SEM analysis of Nuclepore filters behind the LTI found considerably higher concentrations of mineral aerosols than on Nuclepore filters behind the SD and CAI.
- Identical nephelometers found much higher scattering behind the LTI than behind the CAI, and about 13% increase was noted over the SD. Calculations of the non-truncated scattering suggest that the LTI may produce even larger improvements in sampling particles that have a radiative impact.

It should be noted that this conclusion does not address the issue of whether the LTI enhanced particles of any size relative to ambient concentrations. It also does not involve any quantification of the possible ways in which tubing behind the various inlets modified the distributions. Although all the module plumbing was identical between inlets and the large delivery tubes were similar, it is likely that the sharp bend immediately behind the porous diffuser is responsible for its drop in concentrations above 8 μm .

5.2 Comparison of inlets to ambient concentrations

Hypothesis B: *It is possible, using the LTI, to sample and characterize the number-size and surface area-size distributions of ambient dust and seasalt inside an aircraft with enough accuracy that uncertainties arising from inlet losses will contribute less than 20% to the assessment of radiative impacts.*

We conclude that Hypothesis B also cannot be falsified.

Testing Hypothesis B requires comparing aerosols behind the LTI with those in ambient air. The difficulty, of course, involves defining the ambient concentrations. We used evidence from two observational approaches and one model to make that comparison:

- Ion-chromatographic analysis of Teflon filters in TAS showed statistically identical concentrations of Cl^- , Na^+ , Mg^{++} , Ca^{++} , SO_4^- , and NSS[Mg] to those behind the LTI. The net enhancement of the sea salt mode must be less than 10- 20%.
- Scanning electron microscopic counting of particles on Nuclepore filters in TAS showed similar concentrations in size bins up to 2 μm . Above that the LTI concentration exceeded that in TAS by between 20 and 100% at the larger sizes. This argues that some LTI samples show little or no enhancement while others may as much as double the concentration of particles in the 4 to 8 μm range.
- Fluent modeling suggests that the LTI should pass particles with unit efficiency up to several μm . Enhancement above that value may reach 30 - 40% for 6 μm particles. When FLUENT model-derived inertial enhancements associated with the LTI diffuser and losses associated with transport to the LTI filter are taken into consideration, they predict the observed 20% agreement between LTI and TAS.
- We do not yet know the extent to which losses of particles in tubing may offset any enhancement of large particles by the LTI.

We have shown that corrections for modest but predictable LTI enhancements also can produce light scattering assessments that are representative of ambient size distributions up to 7 μm . Additional contributions to scattering from yet larger aerosol are unlikely to approach 20% for realistic aerosol cases. The error in radiative forcing due to positive and negative sampling biases depends both on the transmission efficiency and the fraction of the mass and total optical depth in each size interval. For those sizes that contribute little to the optical depth, a poor transmission efficiency will cause little error in radiative forcing calculations. It is worth noting, however, that over- or under-sampled sizes could still cause significant errors for other issues, such as the computation of deposition fluxes and heterogeneous reaction rates.

5.3 Conclusion and Recommendations

CONCLUSION: Our conclusion, therefore, is that the LTI represents a significant advance in our ability to sample populations of large particles from aircraft. Its efficiency is near enough to unity to enable defensible studies of the distributions and impacts of both mineral dust and sea salt. **Corrections can be applied for the enhancement of particles in the 3-7 μm range.**

Our data suggests that even after estimated enhancements are considered, the LTI shows improved efficiency (closer to unity) for transmission of larger aerosol compared to the SD and particularly the CAI inlets evaluated here. We believe that tubing bends downstream of the LTI compromised this assessments for particles larger than 8 μm , but expect that future versions will have improved transmission efficiencies for these and larger sizes. Scattering extinction measurements behind the CAI were about 40% below LTI values but the SD extinction was only slightly below that of the LTI for this dust aerosol. This reflects the generally reduced impact of larger aerosol on scattering extinction. However, accurate assessment of scattering extinction for larger aerosol require corrections for nephelometer truncation error that will depend upon realistic coarse aerosol measurements. The LTI's improved coarse particle characterization should better constrain radiative assessments of aerosol properties. Studies of other issues related to aerosol character, composition and mass fluxes should also be greatly improved. The LTI's cost (in terms of both system complexity and the weight, power, and heat load from extra pumps) is more than offset by the improvement in large-particle data quality for those programs that need to study supermicron aerosols.

WE RECOMMEND that a modified version of the LTI be used to sample aerosols from the NCAR C-130 during the ACE-Asia experiment. It is important that development work continue on the LTI, to address issues such as losses in tubing and the modeling of enhancements. To make the LTI a practical device its low-altitude sample flowrate needs to be increased and an automated control system must be added.

6. References

- Ananth, G., Wilson, J.C., Theoretical Analysis of the Performance of the TSI Aerodynamic Particle Sizer: The Effect of Density on Response, *Aerosol Sci. Technol.*, 9:189-199, 1988.
- Anderson, J.R., P.R. Buseck, T.L. Patterson, and R. Arimoto, Characterization of the Bermuda tropospheric aerosol by combined individual-particle and bulk-aerosol analysis, *Atmos. Environ.*, 30, 319-338, 1996.
- Bates, T.S., B.J. Huebert, J.L. Gras, F.B. Griffiths, and P.A. Durkee, The International Global Atmospheric Chemistry (IGAC) Project's first aerosol characterization experiment (ACE-1) - Overview, *J. Geophys. Res.*, 103, 16,297-16,318, 1998.

- Baumgardner, D., B. Huebert, and C. Wilson, Meeting Review: Airborne Aerosol Inlet Workshop, NCAR/TN-362+1A, National Center for Atmospheric Research, Boulder, CO, 1991.
- Baumgardner, D., J.E. Dye, R.G. Knollenberg, and B.W. Gandrud, Interpretation of measurements made by the FSSP-300X during the Airborne Arctic Stratospheric Expedition, *J. Geophys. Res.*, 97, 8035-8046, 1992.
- Blomquist, B.W., B.J. Huebert, S.G. Howell, M. Litchy, C. Twohy, D. Baumgardner, B. Lafleur, R. Seebaugh, and M. Laucks, An evaluation of the Community Aerosol Inlet for the NCAR C-130, *J. Atmos. Ocean. Technol.*, in press, 2000.
- Clarke, A.D., J.N. Porter, F.P.J. Valero, and P. Pilewskie, Vertical profiles, aerosol microphysics and optical closure during ASTEX: measured and modeled column optical properties, *J. Geophys. Res.*, Submitted, 1995.
- Gesler, D. (2000) "Numerical Analysis of Sampling Efficiency on a Reduced Turbulence Inlet for Airborne Aerosol Sampling," MSME Thesis, University of Denver.
- Huebert, B.J., G. Lee, and W. Warren, Airborne Aerosol Inlet Passing Efficiency Measurement, *J. Geophys. Res.*, 95 (D10), 16369-16381, 1990.
- Huebert, B.J., S.G. Howell, L. Zhuang, J.A. Heath, M.R. Litchy, D.J. Wylie, J.L. Kreidler-Moss, S. Coeppicus, and J.E. Pfeiffer, Filter and impactor measurements of anions and cations during the First Aerosol Characterization Experiment (ACE 1), *J. Geophys. Res.*, 103, 16,493-16,510, 1998.
- Lachman, G.V. (Editor) (1961) *Boundary Layer and Flow Control*, Pergamon, New York.
- Lafleur, B.G. "A Low Turbulence Inlet for Airborne Aerosol Sampling." University of Denver: MSME Thesis, 1998.
- Marple, V.A. and B.Y.H. Liu. Characteristics of laminar jet impactors, *Environmental Sci. Technol.* 8:648-54, 1974.
- Pui, D.Y.H., F. Romay-Novas, and B.Y.H. Liu, Experimental study of particle deposition in bends of circular cross section. *Aerosol Sci. Technol.* 7:301-15, 1987.
- Rader, D. J., J. E. Brockmann, et al. A method to employ the APS factory calibration under different operating conditions. *Aerosol Sci. and Tech.* 1990, 13:514-521
- Rader, D.J. and V.A. Marple. A study of the effects of anisokinetic sampling. *Aerosol Sci. Technol.* 8(3):283-99, 1988.
- Seebaugh, W.R., and M.E. Childs (1970) "Conical Shock-Wave Turbulent Boundary Layer Interaction Including Suction Effects," *Journal of Aircraft*, Vol. 7, No. 4, pp. 334-340.

- Seebaugh, W.R., B.G. Lafleur, J.C. Wilson, and J. Kim (1997) "Low Turbulence Inlet for Airborne Aerosol Sampling," Patent Disclosure to the University of Denver.
- Seebaugh, W.R., B.G. Lafleur, and J.C. Wilson (1996) "Low Turbulence Inlet for Aerosol Sampling from Aircraft," AAAR Fifteenth Annual Conference, October 14-18, 1996, Orlando, FL.
- Sheridan, P.J., and R.B. Norton, Determination of the passing efficiency for aerosol chemical species through a typical aircraft-mounted diffuser-type aerosol inlet system, *J. Geophys. Res.*, *103*, 8215-8226, 1998.
- Tsai, C.J. and Pui, D.Y.H., Numerical study of particle deposition in bends of circular cross section- laminar flow regime. *Aerosol Sci. Technol.*, *12*:813-831, 1990.
- Wilson, J. C. and B. Y. H. Liu. Aerodynamic particle size measurement by laser-doppler velocimetry. *J. Aerosol Sci.* 1980, *11*:139-150

7. Figures